JOURNAL OF GEOPHYSICAL RESEARCH, VOL. 112, C05046, doi:10.1029/2006JC003779, 2007

Altimetry and drifter data assimilations of loop current and eddies

X.-H. Lin,[1] L.-Y. Oey,[1] and D.-P. Wang[2]

Received 24 June 2006; revised 23 October 2006; accepted 14 December 2006; published 26 May 2007.

[1] The goal is to quantify in an eddy-rich ocean environment the accuracy of currents obtained from a multi-level primitive-equation ocean model that assimilates altimetry sea-surface height anomaly (SSHA) and surface drifters. The 1999–2000 period in the Gulf of Mexico is chosen for the availability of drifters and Acoustic Doppler Current Profiler (ADCP) measurements in the loop current and eddies during that period. Sequential assimilations of SSHA and/or currents with statistical-interpolation schemes are used. Experiments initialized with and without altimetry and/or drifter assimilations, including a forecast case (without assimilation) for comparison, are conducted. It is shown that the SSHA + Drifter analysis consistently outperforms the analysis that assimilates only SSHA, especially at smaller scales. Drifter-assimilation alone also constraints the pressure field, such that the loop and eddies compare quite favorably with altimetry SSH field. When compared against independent ADCP data, the analyses with either SSHA or SSHA + Drifter assimilation yield amplitude and phase of analysis-to-observed complex (velocity) correlation of 0.76∼0.86 and 0.3°∼7°, respectively. The mean speed and direction (absolute) errors are 0.4–5 cm s^{-1} (1∼10% errors) and 10°∼20°, respectively. The correlations of the two dominant empirical orthogonal function (EOF) modes with the corresponding observation modes at a yearlong mooring over the northern slope are: mode-1 $\approx$ 0.88∼0.93 and mode-2 $\approx$ 0.5∼0.63. Both show vertically coherent but strongly sheared modes 1 and 2 representing propagation eddies and reversing mode-3 that intensifies for $z < -300$ m.

Citation: Lin, X.-H., L.-Y. Oey, and D.-P. Wang (2007), Altimetry and drifter data assimilations of loop current and eddies, *J. Geophys. Res.*, *112*, C05046, doi:10.1029/2006JC003779.

1. Introduction

[2] Increased ocean measurements and sophistication in data analysis and modeling techniques are beginning to bridge observations and models. This is particularly true in the Gulf of Mexico where scientific curiosities, commerce, and the needs to protect environments and coastal communities have spurred growths in observations and modeling. By increasing the model's realisms, data assimilation helps blur (in a positive sense) the distinction between observations and models [e.g., *Kalnay*, 2003].

[3] Data assimilation is "the process of combining a physical model with observational data to provide a state analysis of the system which is better than could be obtained using just the data or physical model alone" [*Anderson et al.*, 1996]. When used as initial conditions (in a good model), the analysis should also improve forecasts. In this paper, by forecast we mean an experiment without data assimilation; that is, the forecast needs not be in real time. One way for assessing the "goodness" of the analysis or forecast is to conduct twin experiments (examples are also given in *Anderson et al.* [1996]). In such an assessment, the results from a control run are treated as "observations" which are then used to assimilate into and compared against a different run (initialized differently, say). The advantage is that we then have at our disposal "observations" of every modeled variable in the entire (model) space-time domain. The drawback is that the "observations" and model are not independent of each other. The method is therefore well-suited for testing assimilation schemes but may not produce reliable measures of skill. Another way for skill assessment is to compare the model (either a test-analysis or forecast) against an analysis that is the most complete, thereby treating the latter as "observations." A recent example of this approach is *Miyazawa et al.* [2005]. However, it is clear that this way of skill assessment lessens but does not entirely eliminate the problem of model and observation interdependency. The third way is to use observations to compare with the analysis or forecast [*Wang et al.*, 2003; *Kamachi et al.*, 2004; *Oey et al.*, 2004, 2005a, 2006a, 2006b; *Oke et al.*, 2002; *Paduan and Shulman*, 2004]. Independent observations should be used when assessing the analysis. Clearly, skill assessment against observations is the ultimate way one should judge if an analysis or forecast is any good.

[4] In this paper, we apply data assimilation techniques to produce analyses of currents due to loop current and eddies in the Gulf of Mexico using a multi-level primitive-equation model (see *Sturges and Lugo-Fernandez* [2005] for a collection of recent work and reviews of the circulation in the Gulf;

[1]Princeton University, Princeton, New York, USA.
[2]Stony Brook University, Stony Brook, USA.

0148-0227/07/2006JC003779$09.00

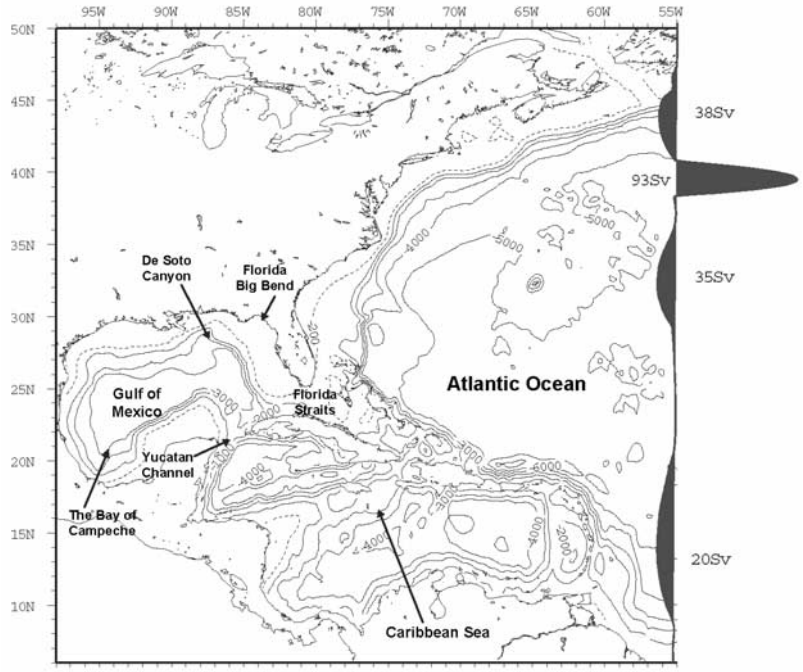

Figure 1. A locator map of the study region: the Gulf of Mexico and surrounding ocean regions. The whole domain shown is also the model domain. Time-independent inflow and outflow that account for the large-scale transports (Svedrup + thermohaline) are specified across the open boundary at 55°W as a function of latitude. Contours show isobaths in m.

Figure 1 shows a regional map with topography). The goal is to evaluate these analyses by assessing their skills against direct observations (the "third way" above). The focus will be on the near-surface currents though sub-surface structures (to about 500 m) will be examined in some cases. We compare the analyses against satellite sea-surface height (SSH), drifter-derived surface currents, and also Acoustic Doppler Current Profiler (ADCP) measurements. An important question is how much improvement one can achieve by assimilating drifter-derived currents in addition to altimetry SSH anomaly (SSHA). The answer is not apparent when using a multi-level Ocean General circulation Model (OGCM). We recognize that advanced data assimilation schemes are presently being developed (see *Bennett* [2002]). However, simple schemes (e.g., statistical interpolation) such as those used here are widely employed for analyses and operational forecasts using the primitive equation models. Our contributions will be in assessing the skills of these schemes and in assimilating drifters to simulate complex mesoscale features. The errors of these simple schemes provide an upper bound that more sophisticated schemes can hopefully reduce.

[5] In section 2, we briefly describe the evolution of the loop current and eddy fields during the study period. Section 3 describes the observations, data assimilation methodologies, the model, and experiments. In sections 4 and 5, the analyses are compared against satellite SSH and drifter-derived surface currents. For some analyses, satellite SSH and drifters clearly do not constitute independent observations. However, they are excellent sets not only for checking the assimilation schemes but also for comparing the different analyses and effects of SSHA and/or drifters on the analyses. In sections 6 and 7, the analyses are assessed against ADCP along the ship-track crossing a newly-shed large eddy and also against a year-long ADCP moored at the northern Gulf slope. The paper ends with a concluding summary in section 8.

2. A Summary of the Loop Current and Eddy Fields

[6] The study period is from Jul/24/1999 through Sep/16/2000. To show the physical conditions that existed in the Gulf during that period, Figure 2 presents daily-averaged currents superimposed on the corresponding SSH on the first of each month for 12 months. The results are from the analysis that assimilates both SSHA and drifters, and the zero-contour from satellite SSH is also shown (see below). The loop current sheds a large ring (Eddy Juggernaut or Eddy-J) in the first 2∼3 months (Figure 2A-C; see also *Oey et al.* [2005a]). After separation, Eddy-J completed a clockwise rotation from Nov/1999 through Jan/2000 (2.5∼3 months; Figure 2C-F) and at the same time drifted west-southwestward about 270 km (drift speed ≈4 km/day; Figure 2D-G). During the first 6 months, the loop current and Eddy-J influence the currents at the Sigsbee mooring (marked "**X**" in Figure 2) where ADCP measurements will be used to assess the model. During the second half of the study period, Eddy-J drifted westward; a portion of Eddy-J merged with an existing weak eddy in the northwestern Gulf (Figure 2G-H). The remaining portion drifted southeastward back into the central Gulf (Figure 2H-I) before propagating into the southwestern Gulf (Figure 2J-L). At the same time, a warm feature was shed from the Loop Current (Figure 2J-L). In the second half of the study period then, currents at the Sigsbee mooring were dominated by fluctuations due to smaller-scale features, including

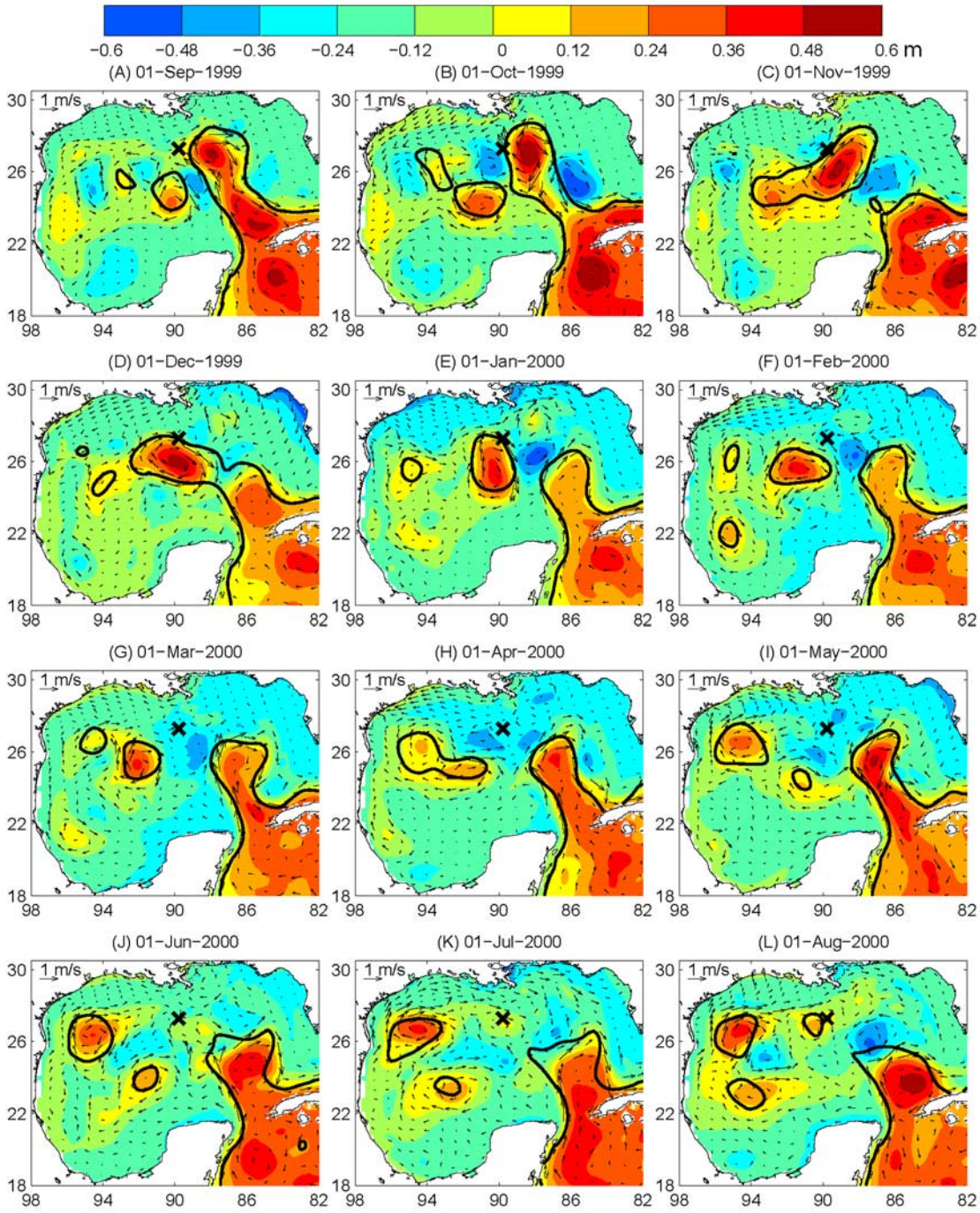

Figure 2. Daily-averaged analysis SSH (color) and surface currents shown on the first of each month from Sep/1999 through Aug/2000 in the Gulf of Mexico. Thick dark contour is the zero-value of satellite SSH (= AVISO SSHA + 10-year model mean). The Sigsbee mooring location is marked with an "x" (see text).

the above-mentioned warm feature in the last 2 months (Figure 2H-L).

3. Methodology

[7] We first describe the observations used for data assimilations and skill-assessments, next the assimilation methods, then the model and various experiments.

3.1. Observations

[8] The observations consist of (i) satellite-derived SSHA maps from the Archiving, Validation, and Interpretation of Satellite Oceanographic data (AVISO) [*Ducet et al.*, 2000], (ii) surface drifters from the Interpolated Global Lagrangian Drifter Database (http://db.aoml.noaa.gov/cgi-bin/db/Bin/init_applet.x?gld+GLDKRIGGUI.class) and from the Minerals Management Service's "Deepwater

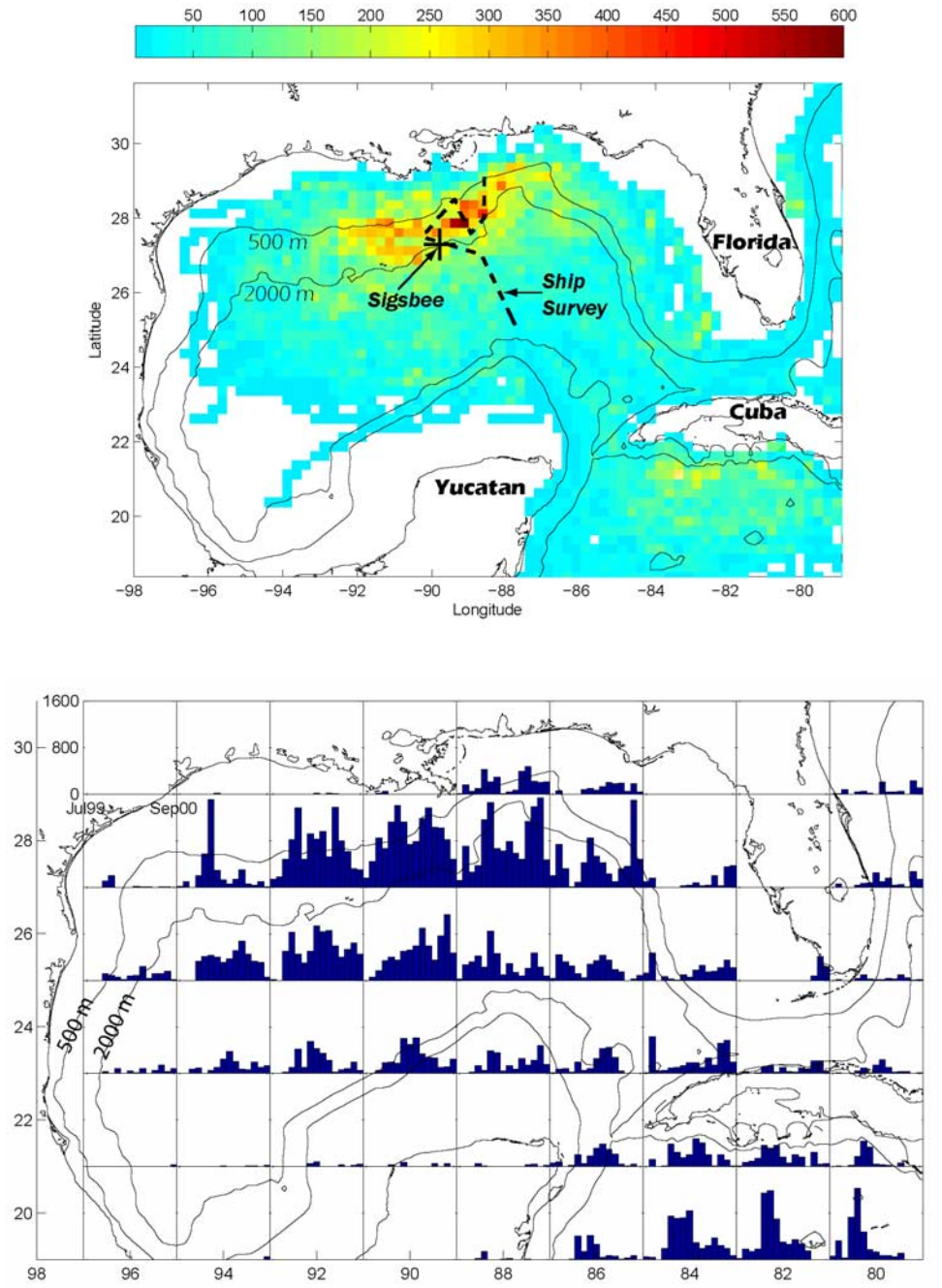

Figure 3. (a) Color shows the drifter density (number of three-hourly drifter observations per 1/4° × 1/4° square from Jul/1999 through Sep/2000). The location of Sigsbee mooring is shown as a '+', and ship's survey (Oct/27–29/1999) is shown as dashed line. Contours show the 500 m and 2000 m isobaths. (b) Monthly number of three-hourly drifter observations within each 2° × 2° square in the Gulf of Mexico, from Jul/1999 through Sep/2000. Top-left most 2° × 2° panel shows abscissa (date) and ordinate (number of observations) values.

Physical Oceanography Reanalysis and Synthesis'' Program (*Nowlin et al.* [2001]; which also includes data collected by Peter Niiler and Carter Ohlmann, e.g., *Ohlmann et al.* [2001]), (iii) ship's ADCP and hydrographic surveys from Texas A&M University (TAMU; *Walpert et al.*, 2004) and (iv) ADCP mooring at Sigsbee from *Hamilton and Lugo-Fernandez* [2001]. The ship's data is from Oct/27 through 29/1999. During this period, the ship measured currents as it crossed the newly-shed Eddy-J. The value of these data is in its spatial coverage providing a snapshot of the eddy. The altimetry data are available from Sep/1999-Sep/2000. The AVISO data product was created by merging TOPEX/Poseidon (T/P) and ERS-1 & -2 altimeter measurements [*Ducet et al.*, 2000]. The combined, intercalibrated

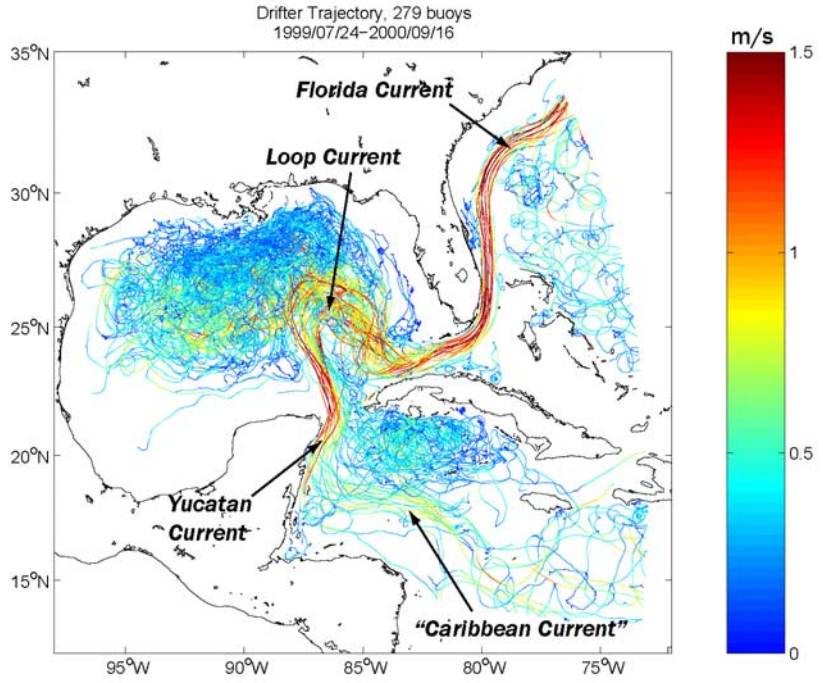

Figure 4. A "spaghetti plot" of all drifter tracks from Jul/1999 through Sep/2000. Colors indicate speeds in m s^{-1}.

altimeter data are interpolated in time and space using a global objective analysis. The length scale of the interpolation varies with latitudes and is about 200 km at mid-latitudes. The e-folding timescale is set at 10 days in the tropics and 15 days elsewhere. The resulting satellite product has a spatial resolution of 1/4° × 1/4° and is provided at 10-day intervals. The merged T/P + ERS-1&2 SSH anomaly maps provide reduced and more homogeneous mapping errors than either of the individual data set and thus more realistic statistics. The AVISO's SSHA maps are bi-linearly interpolated onto the model grid (Figure 1) and also daily in time. Figure 3a shows the spatial distribution of drifter density, the Sigsbee mooring location, and the ship's track. The high concentration of drifters in the northern central slope is due to the relatively large number of initial deployments there (not shown). Positions of the drifters were smoothed using a Gaussian-filter scale of 24 h to eliminate tidal and inertial currents and were sub-sampled at 3-h intervals. The method is given in *Hamilton et al.* [1999]. Velocity components were then estimated from centered finite differences. This pre-processing of drifter data is necessary because the original sampling intervals have gaps as long as 12 hours. To attempt resolving short-period motions due to tidal and inertial currents by assimilating drifter data would be incorrect. Fortunately, tides are weak in the Gulf of Mexico [*Reid and Whitaker*, 1981]. Although inertial currents can be significant, they appear to be primarily wind-driven and generally confined over the shelves and shelf-break [e.g., *Chen et al.*, 1996]. The omission of tidal and inertial motions when assimilating drifters should not therefore seriously compromise our focus of simulating the loop current and eddies. In this work, we limit the model-observation comparisons and their interpretations to subtidal mesoscale eddies. Figure 3b shows the number of sub-sampled 3-hourly data as a function of month; it indicates that most of the drifters are in the northern slope of the Gulf where the number is fairly uniformly distributed from about Oct/1999 through Aug/2000. The ship's ADCP data were not further processed (except for some minor editing for obvious bad data), and only the current field nearest the surface ($z = -44$ m) is used. The Sigsbee ADCP's are moored in the upper 800 m only and consist of six instruments that measure velocity profiles at intervals of either 4 or 8 m. Only data that are complete, Sep/1999-Sep/2000 (except for 3-day service break in the middle), is used in this paper. Thus only four of the six ADCP's are used: three downward-looking from $z = -100$ m, -250 m and -650 m, and one upward-looking from $z = -240$ m. These instruments provide finely-spaced velocity measurements in three ranges: $-106\ \text{m} \geq z \geq -234$ m, $-256\ \text{m} \geq z \geq -336$ m and $-658\ \text{m} \geq z \approx > -1000$ m that we will use to assess the model analyses. Note the wide data gap from -336 m through -658 m. (Details are in *Hamilton et al.* [2003]). The data were smoothed using 36-hour low-pass filter and were sub-sampled at 24-h interval. The Sigsbee mooring is located in a region of energetic meso-scale activities caused by the loop current and eddies (*Hamilton and Lugo-Fernandez* [2001]; also see below). While multiple locations would be ideal, the Sigsbee measurements are nonetheless unique for independent skill-assessment of model analyses of a chaotic eddy field.

3.2. Near-Surface Flow From Drifters

[9] Figure 4 shows a 'spaghetti plot' of all drifter tracks. The Yucatan, Loop, and Florida Currents show up as the only quasi-persistent features, and the current speeds there are strong, about 1∼2 m s^{-1}. We can also see a faint outline of the portion of the "Caribbean Current" in the Cayman Sea [*Fratantoni*, 2001; *Richardson*, 2005]. Of these cur-

Table 1. Available Data (Columns 2–5) for Data Assimilation (DA) and Skill Assessments (SA), and the Various Model Experiments (Rows 2–5)[a]

	Data			
Model Experiments	Altimetry: SSHA (October 1992–Present)	Surface Drifters (July 1999–September 2000)	Ship ADCP and Hydrography (27–29 October 1999)	Current Meter at Sigsbee (September 1999–September 2000)
Forecast	SA	SA	SA	SA
SSHA-DA		SA	SA	SA
Drf-DA	SA		SA	SA
SSHA + Drf-DA			SA	SA

[a]Blank entries indicate data that are not independent when used to compare against the corresponding data-assimilated model runs. The drifter DA consists of various schemes as discussed in the text.

rents, the loop current shows the most variability with large-amplitude vacillations (≈300 km). Flows 'outside' the quasi-persistent currents are clearly more chaotic. In the central and northern Gulf of Mexico, the circulation is a superposition of Loop Current rings and smaller eddies (cf., Figure 2). The current speeds exceed 1 m s^{-1} mostly around rings but are otherwise about 0.2∼0.5 m s^{-1} in most other regions. There is a visual correlation between the high density of observations over the northern central slope in the vicinity of the Sigsbee mooring (Figure 3a) and drifter tracks (Figure 4); the correlation is primarily due to the large number of initial deployments in the northern central slope as mentioned above. Also, only a few drifters were in the southwestern Gulf (the Bay of Campeche) and beyond the outer shelves around the Gulf coast and in the South Atlantic Bight.

3.3. The Assimilation Schemes

[10] The model experiments consist of a test-forecast case (no assimilation) and three analysis cases that assimilate either the SSHA, drifters, or both. The assimilative methods have been described in previous works and are outlined below.

3.4. SSHA Assimilation (SSHA-DA)

[11] We use a slight modification of *Mellor and Ezer's method* [1991; see also *Ezer and Mellor*, 1994]. Satellite SSHA is projected into the subsurface temperature field

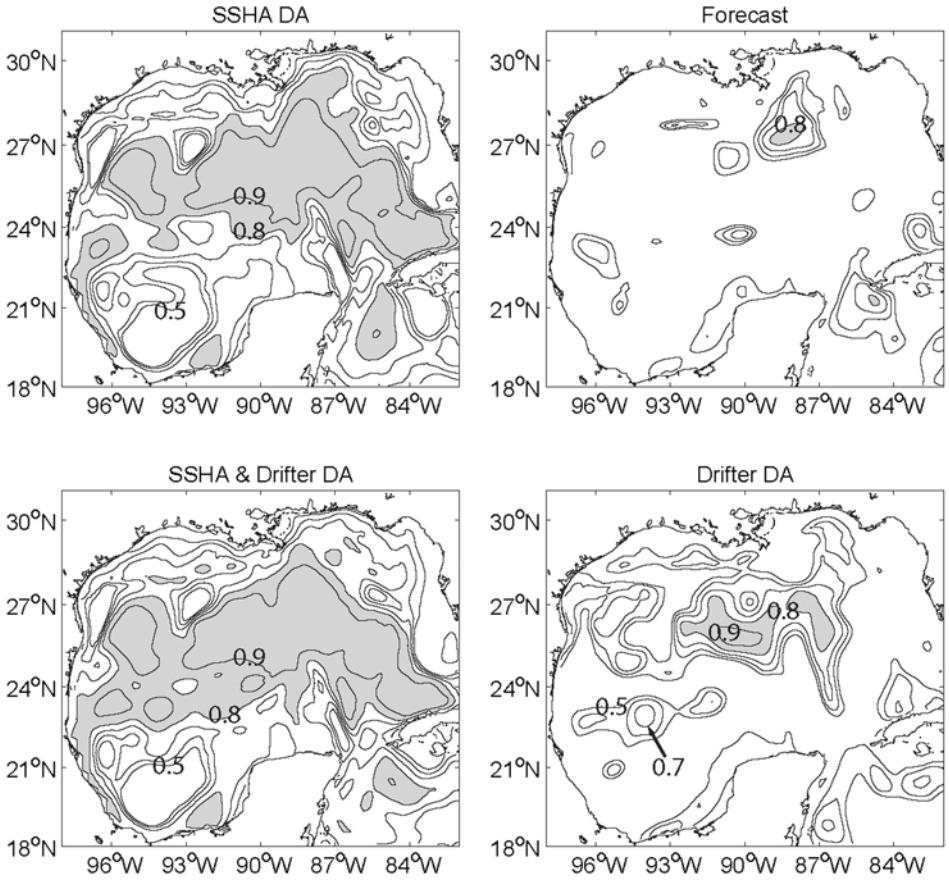

Figure 5. Time correlation (24 July 1999 to 16 September 2000) between analyzed and observed (AVISO) SSHA fields for the four indicated model experiments. Values greater than 0.5 and the 99% significance level are contoured.

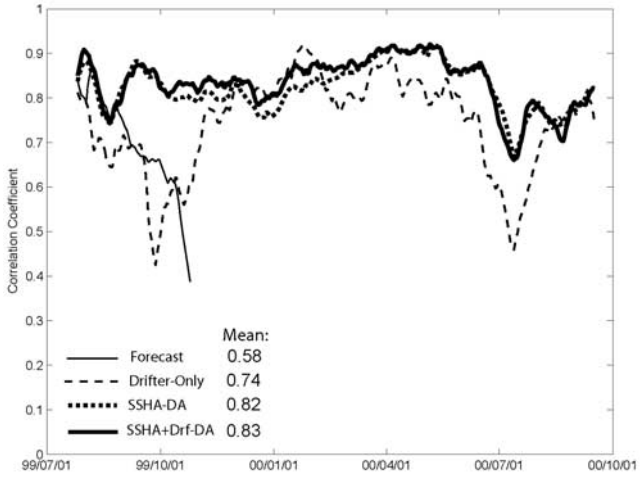

Figure 6. Spatial correlation (north of 23°N, west of 84°W and in water with depths >500 m) between analyzed and observed (AVISO) SSHA fields for the four indicated model experiments. For forecast, only the first 3 months are shown. The mean (over time) correlations are also shown. The 99% significance level is 0.16.

using precomputed correlation functions derived from a long-time (∼10 years) prognostic integration that has yielded a statistical equilibrium eddy field. The resulting temperature anomaly is then added to the observed climatological temperature to yield an estimate of the observed temperature. An Optimal Interpolation (OI) scheme, in which the error covariance matrices are obtained from the above 10-year prognostic integration, then gives the analysis temperature field. We have tested the scheme that assimilates along-track SSHAs [*Mellor and Ezer*, 1991] and also the scheme that assimilates SSHA maps [*Wang et al.*, 2003]. While along-track data are of high (spatial) resolution, there are inherent temporal and spatial scales constrained by times of satellites' overpass and track separation. As a result, the two schemes give very similar assimilated solutions, in agreement with the conclusions of a recent data-assimilative intercomparison exercise using various models of loop current and eddies [e.g., *Oey et al.*, 2005a]. In the following, results from the map assimilation are shown. A similar procedure is carried out using the satellite sea-surface temperature (SST). The SSHA and SST assimilations complement each other: SSHA assimilation is most effective over deep waters (for isobath >500 m), while SST assimilation dominates the analysis field in shallow shelves. For the present application in which the focus is over the deeper water, SSHA assimilation is more important. The modifications to the original Mellor-Ezer's scheme are the use of observed (instead of model) climatology temperature and also a correlation function that depends on SSHA. For more details, see *Wang et al.* [2003], *Fan et al.* [2004], and *Oey et al.* [2005a].

3.5. Drifter Assimilation (DRF-DA)

[12] We directly assimilate velocity $\mathbf{v}_n^o(m)$ computed from drifter positions $\boldsymbol{r}_n^o(m)$, $n = 1, 2, \ldots N$ = number of drifters, at time $t = m\Delta t$, $m = 1, 2 \ldots M$, where Δt is the time step, as:

$$v_n^o(m) = (r_n^o(m) - r_n^o(m-1))/\Delta t \tag{1}$$

Three schemes were tested. The first (Drf-DA1) is identical to *Fan et al.* [2004], and $\mathbf{v}_n^{\mathrm{o}}$ is used as a nudging term in the momentum equation:

$$\frac{\partial \mathbf{u}}{\partial t} = (\text{physics}) - \sum_{n=1}^{N} \lambda_n(\mathbf{u} - \mathbf{v}_n^o)/N \tag{2a}$$

$$\lambda_n = (1/t_{\mathrm{a}}) \exp\left(-r_n^2/R_{\mathrm{nudge}}^2\right) \exp\left(-\left(t - t_n^o\right)/t_{\mathrm{d}}\right) \exp(z/z_{\mathrm{d}}), \tag{2b}$$

where r_n is the distance between the model grid point and the nth drifter's position and $(t - t_n^o)$ is the difference between the model time and the last time when the nth drifter is observed. Nudging is a special case of the standard OI in which the gain matrix is analytically specified (as in here with λ) rather than derived by minimizing the square of the analysis error (*Daley*, 1991). The assimilation timescale t_{a} determines the strength of the nudging factor, and the damping timescale t_{d}, and length scale R_{nudge} are parameters of the nudging term. The $\exp(z/z_{\mathrm{d}})$ term, where $z_{\mathrm{d}} = 10$ m, is used to restrict the effect of the assimilation to approximately the near surface. The t_{d} should correspond approximately to Lagrangian correlation timescale. We use Fan et al.'s values, $t_{\mathrm{d}} = 1$ day, $t_{\mathrm{a}} \approx \Delta t = 675$ s and $R_{\mathrm{nudge}} = 0.4°$. Equation (2) shows that, through the space and time-dependent nudging parameter λ_{n}, model's velocity $\mathbf{u}$ at a grid cell is mainly influenced by the most recent nearby drifters.

[13] The second (Drf-DA2) is *Molcard et al.*'s [2003] and *Ozgokmen et al.*'s [2003] OI scheme:

$$\mathbf{u}^{\mathrm{a}} = \mathbf{u} + \Delta\mathbf{u}, \quad \Delta\mathbf{u} = \alpha \sum_{n=1}^{N} \gamma_n(\mathbf{v}_n^o - \mathbf{u}_n^{\mathrm{b}}), \tag{3a}$$

where $\mathbf{u}^{\mathrm{a}}$ is the analysis vector, and $\mathbf{u}_n^{\mathrm{b}}$ is taken as the model prediction $\mathbf{u}$ interpolated to the drifter location 'n,' and α and γ_{n} are defined as:

$$\gamma_n = \exp(-r_n^2/(2\Delta r^2)) \ \exp(z/z_{\mathrm{d}}), \quad \alpha = \sigma_{\mathrm{b}}^2/(\sigma_o^2 + \sigma_{\mathrm{b}}^2). \tag{3b}$$

Here $\Delta r \approx$ model grid size, σ_{b}^2 is the model velocity mean square error, and σ_{o}^2 is the corresponding error for the observed Lagrangian velocity $\approx \sigma_r^2/\Delta t^2$, where σ_r^2 = mean square drifter position error. Note that we again use z_{d} (=10 m) to limit the velocity assimilation near the surface. We use $\Delta r = n \times$ (grid size) where $n = 5$ and $\alpha = 0.5$. The results are not very sensitive to different values: $1 \leq n \leq 7$ and $0.5 \leq \alpha \leq 1$.

[14] The third scheme (Drf-DA3; *Molcard et al.*, 2003) sets $\mathbf{u}_n^{\mathrm{b}} = \mathbf{v}_n^{\mathrm{b}}$, an estimate of model Lagrangian velocity:

$$\mathbf{v}_n^{\mathrm{b}}(m) = (\mathbf{r}_n^{\mathrm{b}}(m) - \mathbf{r}_n^{\mathrm{b}}(m-1))/\Delta t, \tag{4}$$

where $\boldsymbol{r}_n^{\mathrm{b}}$ is the nth drifter Lagrangian trajectory estimated from the model velocity $\mathbf{u}$ at each time step. The model trajectory is computed using *Awaji et al.*'s [1980] method with a fourth-order Runge-Kutta integration scheme. We have found however that (within the limited parametric range tested) this more sophisticated scheme gives similar measures of improved agreements with (independent)

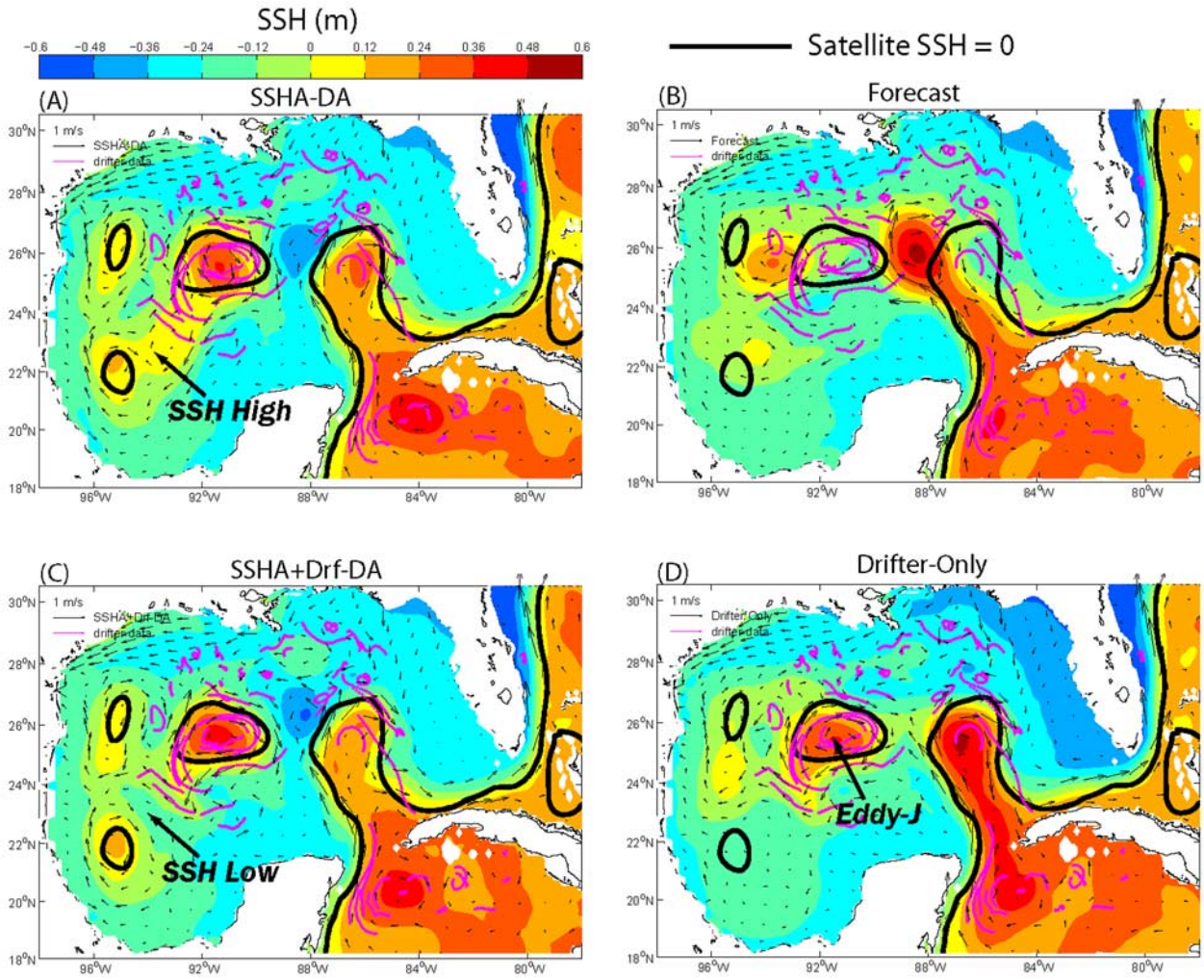

Figure 7. Surface currents superimposed on color SSH maps for (a) SSHA-DA, (b) SSHA + Drf-DA, (c) forecast, and (d) Drifter-only experiments, on 01 February 2000. Thick dark contour is the zero-value of satellite SSH (= AVISO SSHA + 10-year model mean). Seven-day drifter tracks up to 01 February are indicated in magenta.

observations as those obtained from the simpler scheme Drf-DA2 (equation (3)). The scheme Drf-DA2 in turn gives more superior results than the nudging scheme Drf-DA1. In the following, unless otherwise stated, "drifter assimilation" will mean using Drf-DA2.

[15] Equation (2), (3) or (4) updates the near-surface velocities, but the depth-averaged velocities must also be corrected, for otherwise, inconsistencies will arise. We tested two methods. The first is to set the assimilated depth-averaged velocities equal to their original values before the assimilation (i.e., baroclinic adjustments only), and the second is to compute new (i.e., assimilated) values. The two methods did not seem to make much difference probably because the depth-averaged corrections are small, and total integration is relatively short (1 year). Results from the first method only are presented here.

[16] For Drf-DA1, nudging is embedded into the model equation (2), and it is not necessary to separately adjust the pressure field. For Drf-DA2 and 3, two adjustment methods were tested. Method 1 assumes that the model velocities before (i.e., the background) and after (i.e., the analysis) assimilations are in geostrophic balance with their respective SSH (η) field. Taking the difference of the curl then yields a Poisson equation for the correction or perturbation (i.e., analysis minus background) SSH field, η':

$$g\nabla^2\eta' = f\varsigma' - \beta u', \tag{5}$$

where ς' and u' are the perturbation (relative) vorticity and west-east velocity component, respectively, and other symbols are standard. Equation (5) is solved using the Successive Over Relaxation method [*Isaacson and Keller*, 1966] subject to $\eta' \sim 0$ as $r_n \rightarrow \infty$. The subsurface correction is then done by treating η' in the same manner as the altimetry SSHA using the surface-subsurface correlation functions as described previously. In method 2, the primitive equation model itself is used to effect the adjustment. The adjustment is the same as that discussed in *Mellor et al.* [1994; for a different problem], in which perturbations in the velocity yield a modified density field through advection. The adjustment procedure is easily

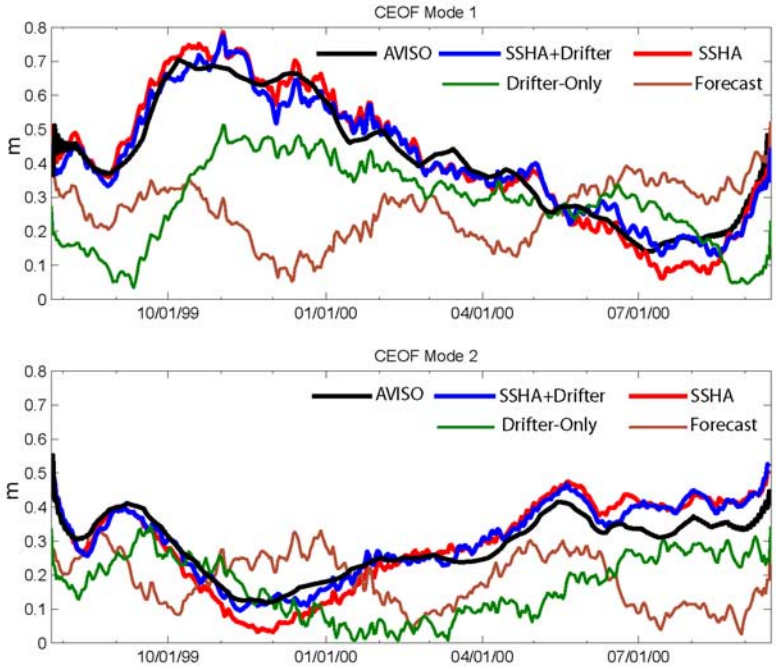

Figure 8. Amplitudes of complex EOF mode 1 (upper panel) and mode 2 for the AVISO and the four indicated model SSH in the Gulf of Mexico (see Figure 9 for the CEOF domain being analyzed).

coded as a separate loop during the model integration. However, we find that, since the perturbations are near the surface and the corrections (u', v') are in the neighborhood of the drifters, the adjustment is localized and relatively fast, within 1–2 days. Therefore, instead of a separate loop for the adjustment, a reordering in the code suffices, such that drifters are assimilated before the density field is updated. The two methods of adjustments give virtually identical results. Since method 2 is more efficient, it is used in the analyses presented below.

[17] In summary, drifters modify the analysis near-surface currents which in turn affect the subsurface current and density fields through advection and geostrophic adjustments. As will be seen below, effects of drifter assimilation are similar to imposing surface stresses.

3.6. SSHA + Drifter Assimilation (SSHA+DRF-DA)

[18] This third analysis case combines SSHA and drifter assimilations. The assimilation begins with Drf-DA every 3 h, then SSHA-DA every 7 days. In summary, the large-scale analysis field is determined by assimilating SSHA (and SST) onto the density field, which modifies **u** (e.g., through geostrophy) and which is refined in local regions by (assimilating) drifters. The combined analysis field $\mathbf{u}^a$ drives (after resetting to **u**) an improved estimate of the temperature and salinity fields and the cycle repeats. *Fan et al.* [2004] showed that the combined scheme gives less (predicted) drifter position errors than the SSHA-DA alone. Though we use different error measures, their conclusion is generally borne out by the present study (below).

3.7. The Model

[19] The model is based on the Princeton Ocean Model [*Mellor*, 2004]. The model domain is shown in Figure 1. At 55°W, estimates of inflow and outflow transports are specified in combination with radiation conditions. The baroclinic velocities are also specified using the radiation conditions, and climatological temperature and salinity are specified during inflow and advected out using one-sided differencing at outflow. Details of open boundary conditions are provided by *Oey and Chen* [1992]. The model is forced by surface fluxes obtained from the European Centre for Medium Range Weather Forecasts (ECMWF), as well as by discharges from 34 rivers along the northern Gulf coast. It has 25 vertical sigma levels and an orthogonal curvilinear grid. The horizontal grid sizes range from about 10 km in the Yucatan Channel to about 5 km in the northern Gulf of Mexico. There are 25 sigma levels in the vertical. In 4000 m of water, the sigma grid cell nearest the surface is at $z \approx -2.8$ m. The model has been used for process studies as well as for realistic simulations [*Oey and Lee*, 2002; *Ezer et al.*, 2003; *Wang et al.*, 2003; *Fan et al.*, 2004; *Oey*, 2004; *Oey and Zhang*, 2004; and *Oey et al.*, 2003a, 2003b, 2004, 2005a, 2005b, 2006a, 2006b].

3.8. Analysis Experiments

[20] There are basically only four experiments (Table 1); all were initialized on 24 July 1999 from a common hindcast field that has been assimilated with SSHA and SST since October 1992 [cf., *Oey et al.*, 2005a], and all ended on 16 September 2000. The forecast experiment has no data assimilation and will be denoted as "forecast." The SSHA-DA experiment assimilates altimetry SSHA (and SST also but this has small effects on the analysis currents over deep waters as mentioned previously). The Drf-DA experiment assimilates only drifters using scheme Drf-DA1, 2 or 3, but only Drf-DA2 is discussed unless otherwise specified as noted previously. Finally, the SSHA + Drf-DA

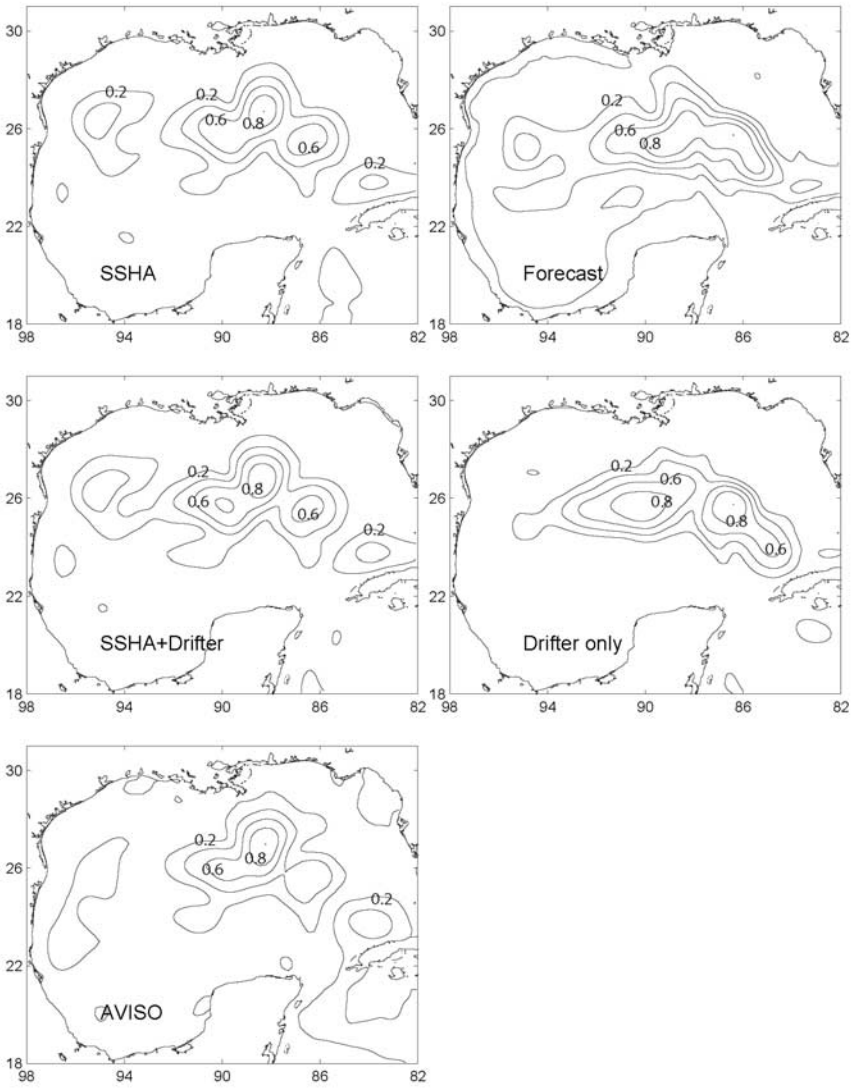

Figure 9. (a) Eigenfunction (normalized) of complex EOF mode 1 for the observed and the four indicated model SSH in the Gulf of Mexico. (b) Same as Figure 9a for mode 2.

experiment assimilates both SSHA and drifters. Again, though analyses using all three schemes were completed, only the case with Drf-DA2 is discussed.

4. Comparisons Between Analyses and Against SSHA Observations

[21] As mentioned previously, the skill of an analysis is ultimately judged based on how well it compares against independent observations. Table 1 clarifies which data sets are independent for which experiments. For example, for the Drf-DA (drifter-only assimilation) analysis, independent data sets are altimetry SSHA, and ship and Sigsbee ADCP measurements. In this section, we intercompare the different analyses using the AVISO data as a yardstick. When interpreting the results, we focus on scales $>\approx$150 km and $>\approx$10 days that are resolvable by AVISO maps. One should be mindful that AVISO is not "truth." The model as well as drifter data can provide information pertaining to the small and fast scales of the real ocean. (An example is hurricane-induced uplifting (depression) of isotherms that can be simulated, and that is also observed as sea-surface depression (uplifting) along satellite tracks crossing the storm's eye, but that is missed by AVISO maps [*Oey et al.*, 2006b]. Another example is frontal eddies in northeastern Gulf of Mexico [*Wang et al.*, 2003; *Fan et al.*, 2004]). On the other hand, the larger scale eddies and loop current generally contribute to a substantial portion of the open-ocean eddy energy. As we will see, the drifter-only assimilative analysis also retains this dominant larger scale signal.

[22] Figure 2 shows that the observed (AVISO) SSH = 0 contours (dark lines) coincide quite well with the frontal lines that separate warm (red) and cooler (blue-green) waters seen in the SSHA + Drf-DA analysis. While the good match is to be expected for a model that assimilates SSHA, comparisons with observed SSH can yield useful

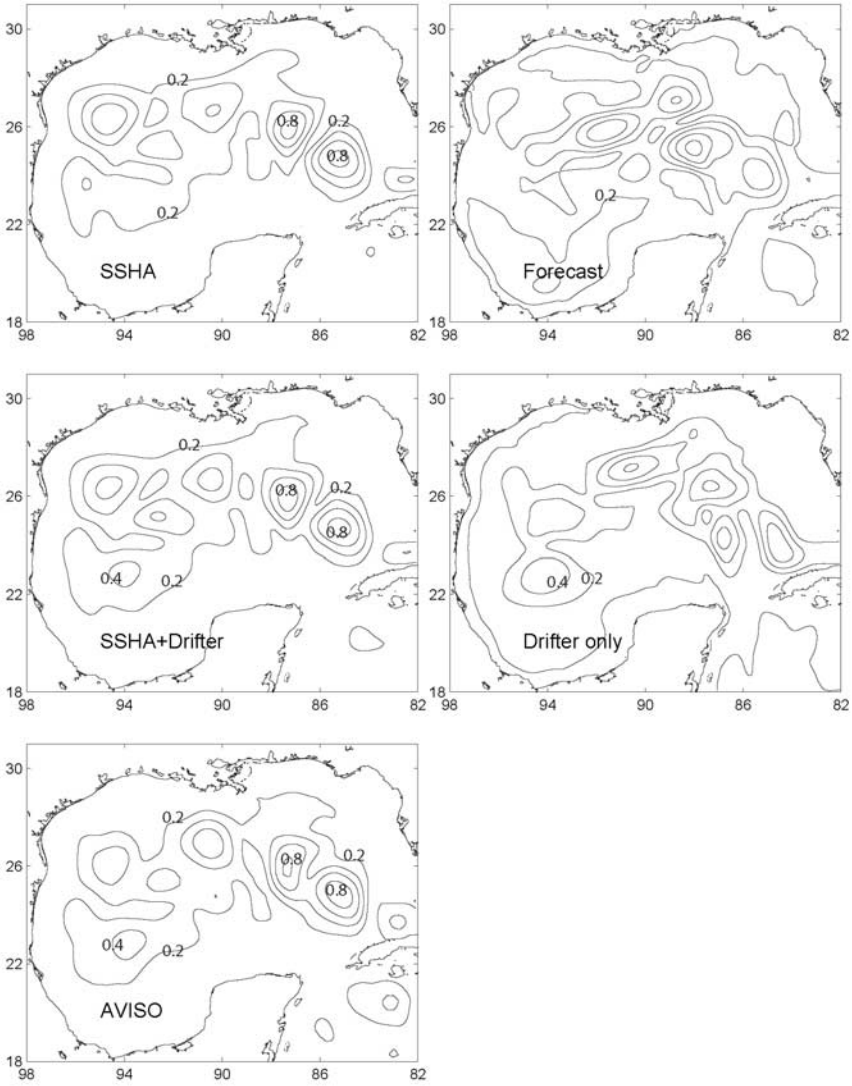

Figure 9. (continued)

information on the model's behaviors when drifters (by themselves or in conjunction with SSHA) are assimilated or when the model is free-running (i.e., forecast). A key question is how assimilating drifters can improve the analysis field. A measure of closeness of match between AVISO and modeled SSH is obtained by calculating their correlations. Figure 5 shows spatial maps of time correlations for the four experiments: SSHA-DA, SSHA + Drf-DA, forecast, and Drf-DA. It shows that SSHA-DA and SSHA + Drf-DA yield similarly high correlations (>0.8) across the central northern Gulf (>≈24°N) in the loop current and over the west Florida slope. There are local regions where assimilating drifters decrease (in the De Soto Canyon) or increase (near 23°N in the southwestern Gulf) the correlations. In the De Soto Canyon, the model attempts to simulate smaller scale eddies depicted by drifters but not by AVISO (cf., *Fan et al.*, 2004). Comparing the forecast and Drf-DA cases in Figure 5 clearly shows that including drifters improves the analysis. While the forecast case shows low or insignificant correlations over a large portion of the Gulf, the Drf-DA case shows high correlations over the north-central Gulf, a region with high concentration of drifters (Figure 3). Significant and fairly high correlations (0.5–0.7) are also seen near 23°N in the southwestern Gulf, in the northwestern Gulf, and also along the Louisiana-Texas (LATEX) slope. In the southwestern Gulf, it is clear that assimilating drifters contributes to the improved SSHA + Drf-DA analysis when compared with the SSHA-DA analysis, as noted previously.

[23] Instead of temporal correlations (Figure 5), spatial correlations indicate how well the locations of simulated eddies and loop current match AVISO. Figure 6 shows the time series in the region north of 23°N and west of 84°W and in open seas where water depths >500 m. This is a region where eddies and vacillations of loop current are prominent. For the forecast, the correlation is only meaningful (and therefore shown) for the first 3 months, which

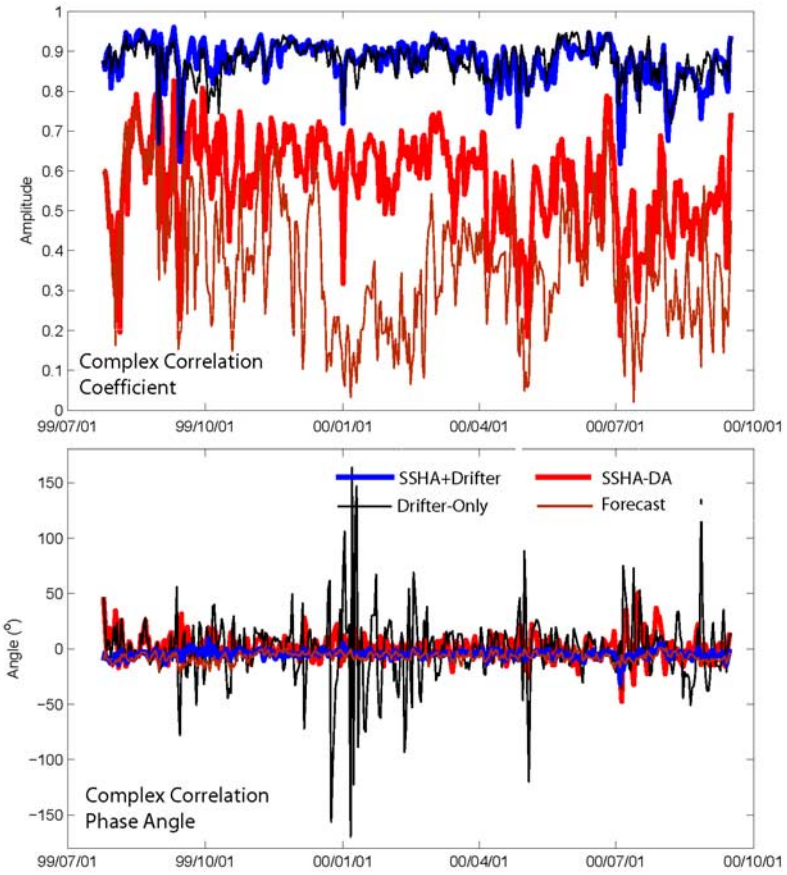

Figure 10. Complex correlations (CC) between the velocities from four indicated analysis (and forecast) experiments and drifter-derived velocities. The CC is computed at each time over all drifters and then plotted as a function of time from August 1999 through September 2000.

is approximately the period of predictability of our model (*Yin and Oey*, 2007). A high correlation (≈0.9) indicates a near-perfect match of model and AVISO eddies and loop current, as for example near 01 February 2000. The correlation drops at the other extreme when the loop and/or eddies misalign as for example in August 2000 (cf., Figure 2). The 01 February 2000 example is shown in Figure 7 as SSH color images for the four cases, and superimposed on them are the corresponding surface currents, the SSH = 0 contours from AVISO, and 7-day drifter tracks. Note that the two fields (a) SSHA-DA and (b) SSHA + Drf-DA are similar except that, in the former case, the small warm eddy in the southwestern Gulf is connected with the main eddy in the central Gulf by a region of high SSH (as indicated), but in the latter case, the two eddies are not connected. AVISO SSH indicates two disconnected eddies (thick dark contours). Thus drifters that originally were in the main eddy appeared to have remained in that eddy throughout the assimilation period. It is clear that the drifter assimilation scheme constraints Eddy-J so it remains disconnected from the small eddy. The effects of assimilating drifters are unambiguously seen by comparing (c) the (6-month) forecast with (d) the analysis that assimilates only drifters. Two major differences can be seen. First, the position and orientation of the model

Table 2. Mean and Standard-Deviation (Std) Errors of Speeds and Directions for the Four Indicated Model Experiments When Compared Against Surface Drifter-Derived Velocities[a]

	Speed Errors				Direction Errors				CC	
Model Experiments	Mean, m/s	R_m	Std, m/s	R_{std}	Mean, deg	R_m	Std, deg	R_{std}	A_{CC}	θ_{CC}, deg
Forecast	−0.053	0.17	0.061	1.0	6.7	–	24.4	1.26	0.37	−0.2
Drifter Only	−0.018	0.06	0.021	0.35	2.3	–	12.9	0.66	0.87	−7.3
SSHA	−0.025	0.08	0.051	0.85	−1.1	–	24.6	1.27	0.60	1.2
SSHA and Drifter	−0.013	0.04	0.021	0.35	1.4	–	13.0	0.67	0.88	−5.1

[a]Amplitude (A_{CC}) and phase angle (θ_{CC}) of the complex correlation (CC) for all the drifters are also shown. Positive "Ang" means that the model is rotated anticlockwise from observation. R_m = |mean error|/(observed Mean) and R_{std} = (Std Error)/(observed Std). The observed (mean, Std) are (0.31, 0.06 m s^{-1}) for speed, and are (0.7°, 19°) for direction.

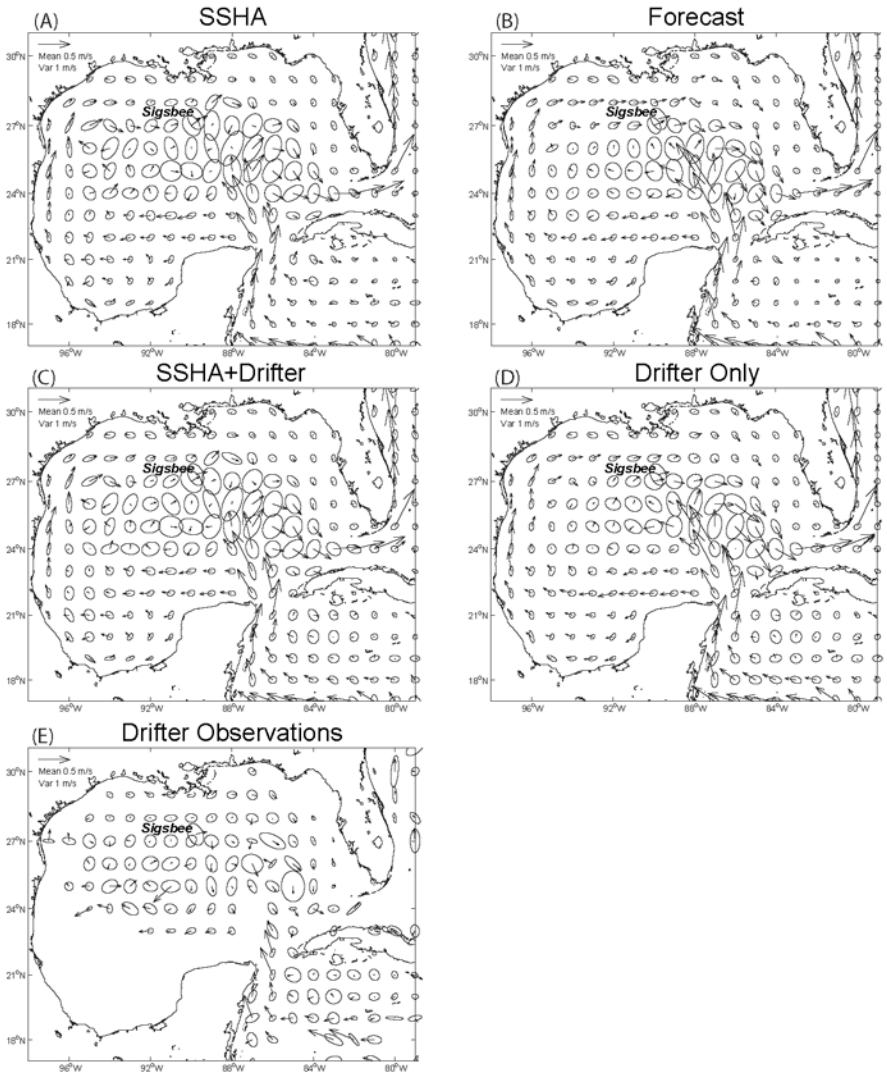

Figure 11. Mean velocity and principal axis standard deviation ellipses for the four indicated analyses and for the drifter observations in $1 \times 1^{\circ}$ squares. The period is July 1999 through September 2000. For comparison, each plot also shows the mean and ellipse at the Sigsbee mooring (90°W, 27.25°N; Figure 3a). See text for details.

loop current in Figure 7d agree well with the analyses that include SSHA assimilation (Figure 7a or 7c) and also with satellite SSH. In the forecast case (Figure 7b), the loop current's orientation is significantly different. Second, the forecast Eddy-J has moved farther to the west than both the SSHA-assimilative analysis and AVISO. By contrast, the drifter-only assimilative analysis (Figure 7d) retains the correct position of the eddy. We find in fact that the model loop sheds eddy only once (Eddy-J; as in observation, see, e.g., *Oey* [2004]; we do not count the small and very weak eddy shed near the end, see Figures 2j, 2k, and 2l) during the study period for all the analyses expect the forecast case which sheds two more eddies after Eddy-J. It is quite remarkable that (in a multilevel model) assimilating near-surface drifters alone can constraint the loop current and eddies.

[24] Another way for skill assessment is to intercompare complex empirical orthogonal functions (CEOFs) which are apt for examining (predominantly unidirectional) propagating signals [e.g., *Merrifield and Guza*, 1990]; the dominant modes presumably also portray larger scale eddy signal. However, as mentioned previously, Eddy-J was more erratic involving rotation and westward propagation (Figures 2b, 2c, 2d, 2e, 2f, and 2g), eddy splitting, merging and stalling (Figures 2h, 2i, and 2j), and finally southwestward propagation (Figures 2j, 2k, and 2l). The CEOF phases show these complex patterns (not shown). We compare instead modes 1 and 2 amplitudes in Figure 8 and the corresponding eigenfunctions in Figure 9. The first mode explains about 50% of the total variance, and the second mode explains 25%. Not surprisingly, both modes from SSHA-DA and SSHA + Drf-DA agree well with AVISO (labeled "observed"; Figure 8). The mode 1 has a maximum near end of October indicating shedding of Eddy-J. It also increases toward the end, but no eddy was shed; instead the loop current extended northward

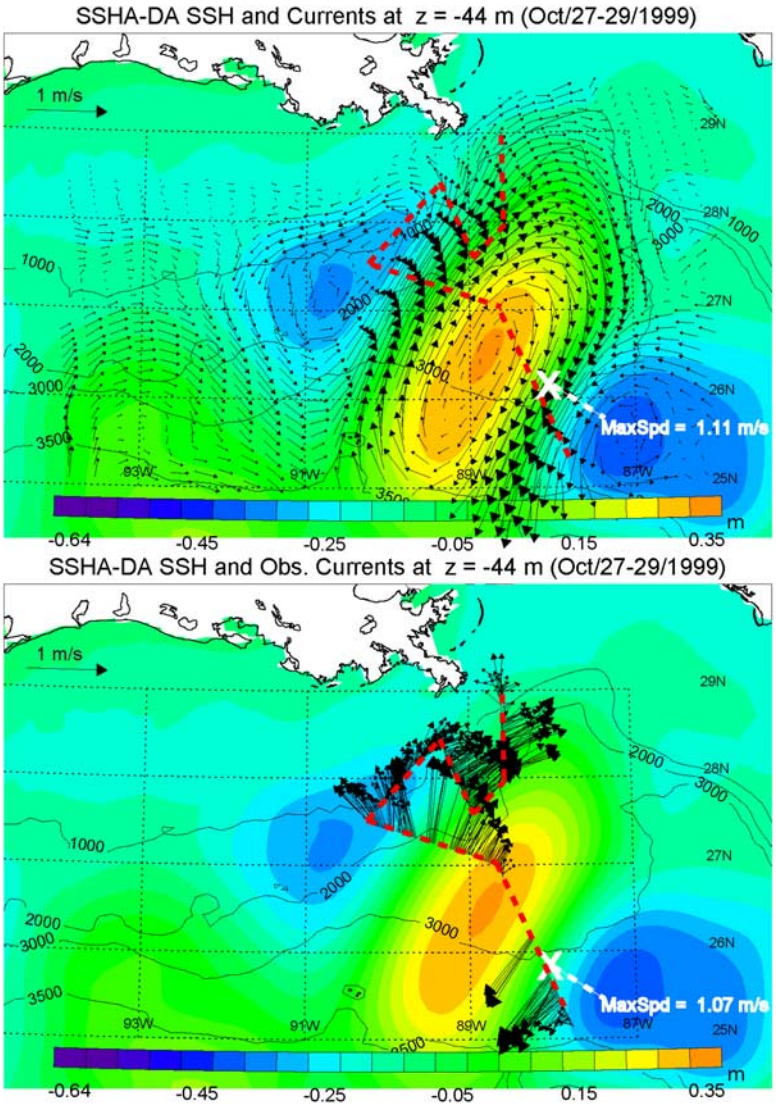

Figure 12. Analysis (upper panel; SSHA-DA) and along-ship track observed (lower panel) currents at $z = -44$ m superimposed on the analysis SSH (color). Tails of observed vectors are on the ship track indicated by red dashed line. Locations and values of maximum speeds are indicated at the "**X**" point.

[*Oey*, 2004]. The Drf-DA modes are correlated with AVISO (more so for mode 1), but the amplitudes are smaller. The forecast mode 1 also has a maximum (eddy shedding) near end of October, but it indicates two other maxima (also shedding), one in March and another one in June 2000. Therefore, while the forecast successfully *predicted* the first shedding (a 3-month forecast), the intensity is weaker, and thereafter, the solution bears no resemblance to the other analyses. All model analyses also contain shorter period (5–10 days) oscillations that are absent from the AVISO time series, since the latter is smoothed (see above).

[25] Mode 1 eigenfunctions for SSHA-DA and SSHA + Drf-DA are virtually identical (Figure 9a), and both are very similar to the AVISO mode 1 except in the northwestern Gulf where AVISO is weaker. In the loop current, there are two maxima separated by a trough which indicates the predominant location of the cyclone either during loop current separation or after Eddy-J has separated. The cyclone (as well as the loop and Eddy-J) in the forecast is much weaker resulting in a more diffused mode 1. The Drf-DA mode 1 is intermediate, the trough exists though the loop current, and Eddy-J does not extend as far north as in the SSHA-DA or SSHA + Drf-DA. Mode 2 eigenfunctions for SSHA-DA, SSHA + Drf-DA, and AVISO are also similar and show finer scale structures (Figure 9b). The AVISO mode 2 structure is more similar to SSHA + Drf-DA: high in the southwestern Gulf and also the joined double-cell (peanut shape) in the loop current. Mode 2 from Drf-DA shows the southwestern high but otherwise has little resemblance with AVISO. As noted above, the good match in the southwestern Gulf between SSHA + Drf-DA and AVISO is as much due to the absence of drifters there (south of approximately the 24°N; Figure 4) as due to the presence of drifters further

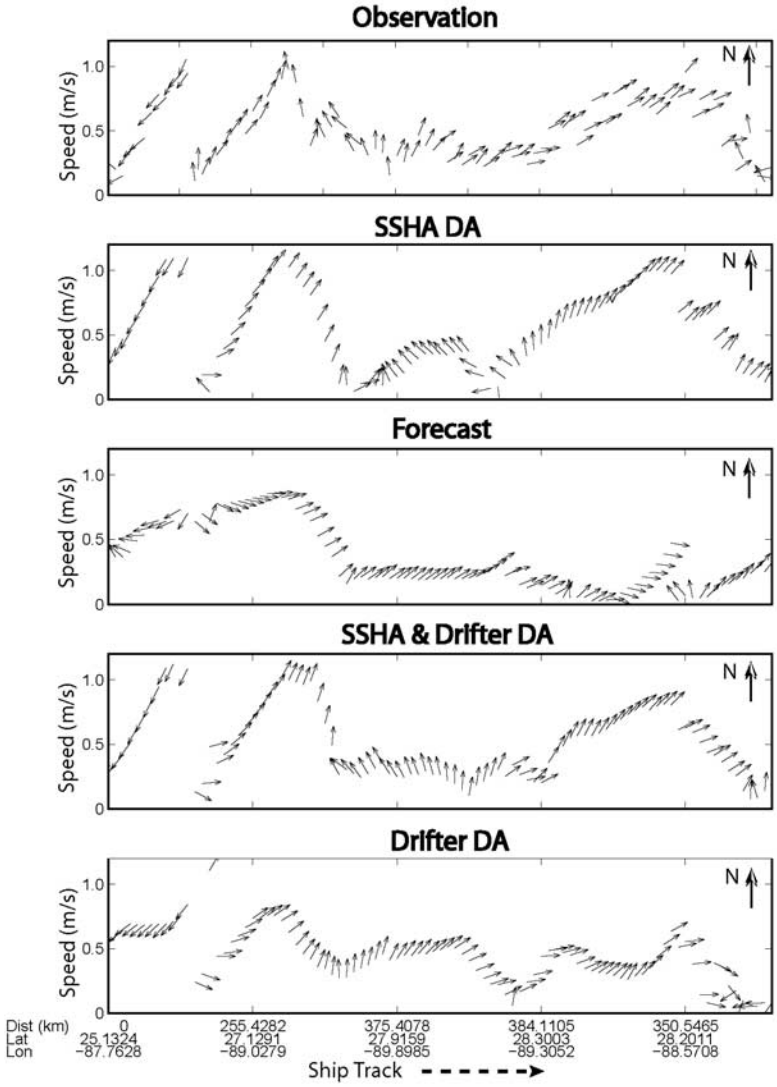

Figure 13. A comparison of ADCP velocity at $z = -44$ m (''observation'') along the ship track with the four indicated model experiments. Each velocity is plotted as a constant length arrowed vector that indicates direction, and the ordinate value of its tail indicates speed.

north. For the forecast mode 2, fine-scale structures exist but they bear little resemblance with the AVISO mode 2.

5. Comparisons Against Drifter Observations

[26] The four cases above are also compared against currents computed from drifters. The complex correlation (CC; see Appendix) of modeled and observed velocities over all the drifters is computed, and its amplitude and angle as a function of time are given in Figure 10. Table 2 summarizes the results in terms of mean and standard deviation (Std) errors and also time-averaged complex correlation. For a model analysis to be any good, we require $|CC| \approx 1$ and small θ_{CC}. For SSHA + Drf-DA and Drifter-only DA, comparison against drifters does not represent an independent skill assessment, but it serves as a check of the drifter assimilation scheme. The $|CC|$ for these two cases is high, and the θ_{CC} is small (Figure 10). The Std errors are within the observed Stds (Table 2). For SSHA-DA, the errors (mean and Std) are approximately doubled, and $|CC|$ is reduced (≈ 0.6). However, the %errors are still quite small, and θ_{CC} is also small. For the forecast, the errors further increase, and the low $|CC|$ and Figure 10 suggest that the model looses its predictability in about 3 months. As in the case of Figure 6, the forecast plots for time $> \approx 3$ months are therefore not meaningful but are included for comparison. Interestingly, there is a negative angle bias for the analyses that assimilate drifters, indicating that modeled current vectors are consistently clockwise from the drifters' paths. This suggests that the effect of drifter assimilation is similar to applying a surface stress which tends to induce a clockwise veering of velocity with depth.

[27] We now compare mean currents and principal axis Std (PAStd) ellipses within $1 \times 1^\circ$ squares computed from the model and the drifter observations (Figure 11). The mean and PAStd ellipse calculated from the 1-year ADCP time series at $z = -106$ m at the Sigsbee mooring are also shown. For the model, (u, v) grid values (at a given time)

Table 3. Mean and Standard-Deviation (Std) Errors of Speeds and Directions for the Four Indicated Model Experiments When Compared Against Ship ADCP Data at $z = -44$ m[a]

	Speed Errors				Direction Errors				CC	
Model Experiments	Mean, m/s	R_m	Std, m/s	R_{std}	Mean, deg	R_m	Std, deg	R_{std}	A_{CC}	θ_{CC}, deg
Forecast	−0.15	0.30	0.30	1.3	−18.3	–	77.4	1.1	0.58	−54.2
Drifter Only	−0.07	0.14	0.23	1.0	−32.9	–	64.5	0.9	0.78	−15.3
SSHA	0.05	0.10	0.18	0.8	9.1	–	67.1	0.9	0.77	6.7
SSHA and Drifter	0.01	0.02	0.17	0.7	4.8	–	48.5	0.7	0.86	4.3

[a]Amplitude (A_{CC}) and phase angle (θ_{CC}) of the complex correlation (CC) along the ship track are also shown. Positive "Ang" means that the model is rotated anticlockwise from observation. R_m = |mean error|/(observed mean) and R_{std} = (Std error)/(observed Std). The observed (mean Std) are (0.5, 0.23 m s^{-1}) for speed, and are (35°, 72°) for direction. The R_m for direction is not meaningful and is omitted.

within each square are averaged to construct time series; the results are not significantly changed if bilinear interpolations to the center of each square are used instead. For observation, (u, v) values from all drifters (at a given time) within each square are averaged. The resulting time series (for each square) is used in the analysis only if it is contiguous for at least 10 days, which is approximately the upper bound of timescale of the synoptic wind forcing. If there are more than one such time series, weighted ensemble average (weighted by the length of each series) of the means and ellipses is then used. A more extensive statistical treatment is probably not warranted for the relatively short-time drifter observations used here.

[28] Some general comments can be made (Figure 11). Firstly, the observed means and ellipses in some regions clearly do not represent the long-term circulation, e.g., in the loop current where the flow seems ambiguous and also near 91°W, 25°N, where the southwestward vector is excessively large (Figure 11e). The latter is because there were only few drifters, while in the loop current, the flow is so strong that the number of samples is effectively reduced. Secondly, the model Stds have similar magnitudes as those observed for both the assimilated runs and the forecast. The exception is in the Caribbean Sea, where the forecast (Figure 11b) and SSHA-DA (Figure 11a) show much weaker variability than observation (Figure 11e), but including drifters improves the analysis (Figures 11c and 11d). Thirdly, westward currents along 17–18°N in the Caribbean Sea and intensified northward flow along the Yucatan coast prevail in the model as well as observation. Fourthly, model analyses produce a more well-defined anticyclonic mean gyre than observed, especially for forecast (Figure 11b). The westward currents along 22–24°N in the Gulf agree with observation and appear also in long-term (∼10 years) drifter analysis by *DiMarco et al.* [2005], who attributed the currents to wind and the westward flows induced by loop current eddies. However, though northward currents are observed in the northwestern Gulf, the eastward "return" flow in the north (along 27–28°N, within 90–95°W) is erratic and very weak (Figure 11e), consistent with the fact that small-scale eddies (diameters <≈150 km) populate this region [*Hamilton*, 1992; *Oey et al.*, 2003b; *DiMarco et al.*, 2005]. A higher resolution model is required to more correctly simulate small eddies [*Oey et al.*, 2003b], though assimilating SSHA and/or drifters appears to rectify the problem in that both (Figures 11a and 11c) show weakened currents (when compared with the forecast case) especially along the LATEX slope. On the other hand, the modeled mean and Std ellipses compare favorably with the observation at Sigsbee; both show an eastward mean of about 0.1 m s^{-1}, i.e., in anticyclonic sense. (ADCP data at $z \approx -10$ m (instead of −106 m) available only for the first 5 months give similarly strong eastward

Table 4. Same as Table 3 for Comparison Against Sigsbee ADCP Velocities at the Indicated Depths[a]

		Speed Errors				Direction Errors				CC	
Model Experiments	z, m	Mean, m/s	R_m	Std, m/s	R_{std}	Mean, deg	R_m	Std, deg	R_{std}	A_{CC}, deg	θ_{CC}
Forecast	−106	−0.084	0.23	0.246	1.0	−16.4	–	10.5	0.15	0.55	−7.6
	−150	−0.039	0.13	0.205	1.13	−58.0	–	32.3	0.44	0.54	−2.8
	−300	−0.015	0.09	0.123	1.1	17.5	–	7.6	0.09	0.55	2.7
	−658	0.002	0.03	0.051	1.2	−93.6	–	8.4	0.09	0.31	−18.0
Drifter Only	−106	−0.136	0.38	0.186	0.71	−58.5	–	15.8	0.22	0.62	−10.0
	−150	−0.112	0.39	0.146	0.80	−61.3	–	10.5	0.14	0.57	−12.4
	−300	−0.073	0.46	0.104	0.94	93.3	–	11.8	0.15	0.50	−19.9
	−658	0.002	0.03	0.057	1.32	−108.	–	15.1	0.16	0.30	−25.0
SSHA	−106	−0.009	0.025	0.191	0.8	−13.9	–	8.9	0.13	0.80	3.9
	−150	−0.032	0.11	0.185	1.0	22.2	–	14.5	0.2	0.76	6.6
	−300	0.054	0.34	0.136	1.23	0.1	–	17.9	0.22	0.70	11.5
	−658	0.085	1.21	0.061	1.42	−110.	–	14.4	0.15	0.41	20.3
SSHA and Drifter	−106	−0.004	0.011	0.165	0.69	−12.9	–	11.9	0.17	0.85	0.3
	−150	0.032	0.11	0.167	0.92	10.2	–	16.6	0.22	0.81	1.9
	−300	0.051	0.32	0.113	1.02	−29.5	–	12.7	0.16	0.74	6.0
	−658	0.073	1.04	0.067	1.6	−147.	–	22.5	0.24	0.40	14.7

[a]The observed (mean, Stds) at z = [−106, −150, −300, −658 m] are [(0.36, 0.24), (0.29, 0.18), (0.16, 0.11), (0.07, 0.04) m s^{-1}] for speed and are [(13°, 71°), (14°, 73°), (18°, 81°), (11°, 94°)] for direction.

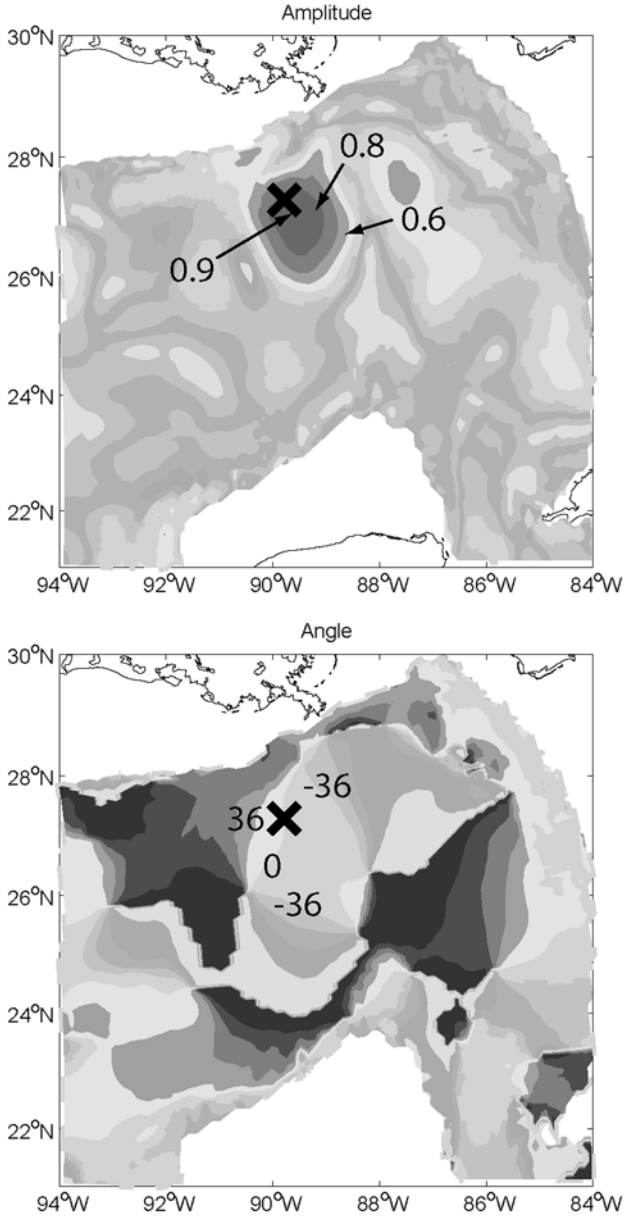

Figure 14. Vector correlation between observed current at Sigsbee (marked as a cross) at $z = -106$ m and SSHA-Drf-DA analysis currents in the domain shown. Upper panel shows the correlation coefficient and lower panel the correlation angle (degrees).

mean.) By comparison, the drifter analysis (observation) near the Sigsbee mooring gives a weak eastward mean of only 0.03 m s^{-1} and a weaker (by about 50%) Std ellipse. This discrepancy is puzzling considering that drifter data near Sigsbee appear to be sufficient both in the total number and also in temporal coverage (Figure 3b). It may suggest the dominance of shorter spatial scales (smaller than the $1 \times 1^\circ$ square). Finally, *Vázquez de la Cerda et al.* [2005] have observed the existence of a cyclonic circulation in the southwestern Gulf of Mexico (Bay of Campeche) and attributed the feature to forcing by the regional wind stress curl. Our model was forced by the ECMWF wind stress. However, the drifter-only analysis and the forecast (Figures 11b and 11d) do not reproduce the cyclone. On the other hand, both the SSHA-DA and SSHA + Drf-DA analyses (Figures 11a and 11c) show the cyclonic feature, and the SSHA assimilation therefore appears to have corrected the model deficiency. Future work could focus on a more detailed analysis necessary to isolate the wind forcing.

6. Skill Assessment Against Ship Track ADCP Across Eddy-J

[29] At the beginning of the study period (August 1999), the loop current was in a north-northwestward extended position, on the verge of shedding an eddy. Approximately 2 months later (~October 20), Eddy-J separated from the loop current (Figures 2a, 2b, and 2c). TAMU ship survey was made across the eddy from 27–29 October. Figure 12 compares the ADCP measurements at $z = -44$ m with the SSHA-DA analysis currents; in both cases, vectors are superimposed on the analysis SSH. Gaps in observed vectors indicate missing data. Eddy-J is clearly seen in this figure. There is an approximate correspondence between the two velocity fields, including the location and value of the maximum speed southeast of Eddy-J. Here strong currents are caused by the presence of a cyclone between Eddy-J and the loop current after shedding (cf., *Schmitz*, 2005; see also Figure 2c). Northwest of the eddy, observed vectors turn anticlockwise consistent with the existence of a cyclone seen in the analysis, though the turning in the modeled vectors is less. The agreements are not good near the end of the survey due east of the Mississippi Delta where observed currents display smaller scale structures. These small-scale features may reflect the effects of the Mississippi River plume and perhaps also its interaction with the wind. Although climatological monthly discharges are included in the model, plumes are notoriously difficult to simulate due in part to our lack of understanding to model turbulence in highly stratified environments [e.g., *Garvine*, 1999]. Figure 13 compares the observed and modeled stick vectors along the ship track, for the same four cases analyzed in the previous sections: SSHA-DA, forecast, SSHA + Drf-DA and Drf-DA. The plot (Figure 13) displays clearly both speeds and directions and eliminates vector crossings and ambiguous speeds that often plague the more conventional 'stick plots.' The forecast in Figure 13 is a 3-month forecast; although it correctly predicts the shedding of an eddy (section 4), the position of the eddy does not coincide perfectly with Eddy-J. The mismatch shows up as errors both in direction and speed (weaker) along the ship track. With SSHA-DA, the general velocity variation along the ship track is reproduced, as noted above. The result is improved when drifters are also assimilated (SSHA + Drf-DA), as can be seen from the corresponding plot in which some details in the velocity variation are visibly improved; e.g., in the middle of the survey and also toward the end. Table 3 gives a quantitative summary of the errors in terms of mean and standard deviation as well as the complex correlations between the observed and model velocities. The amplitude (A_{CC}) and phase angle (θ_{CC}) of the complex correlation between forecast and observation, CC (forecast), are 0.58 and -54°, respectively. When drifters are assimilated, the A_{CC} (Drifter-only) is improved,

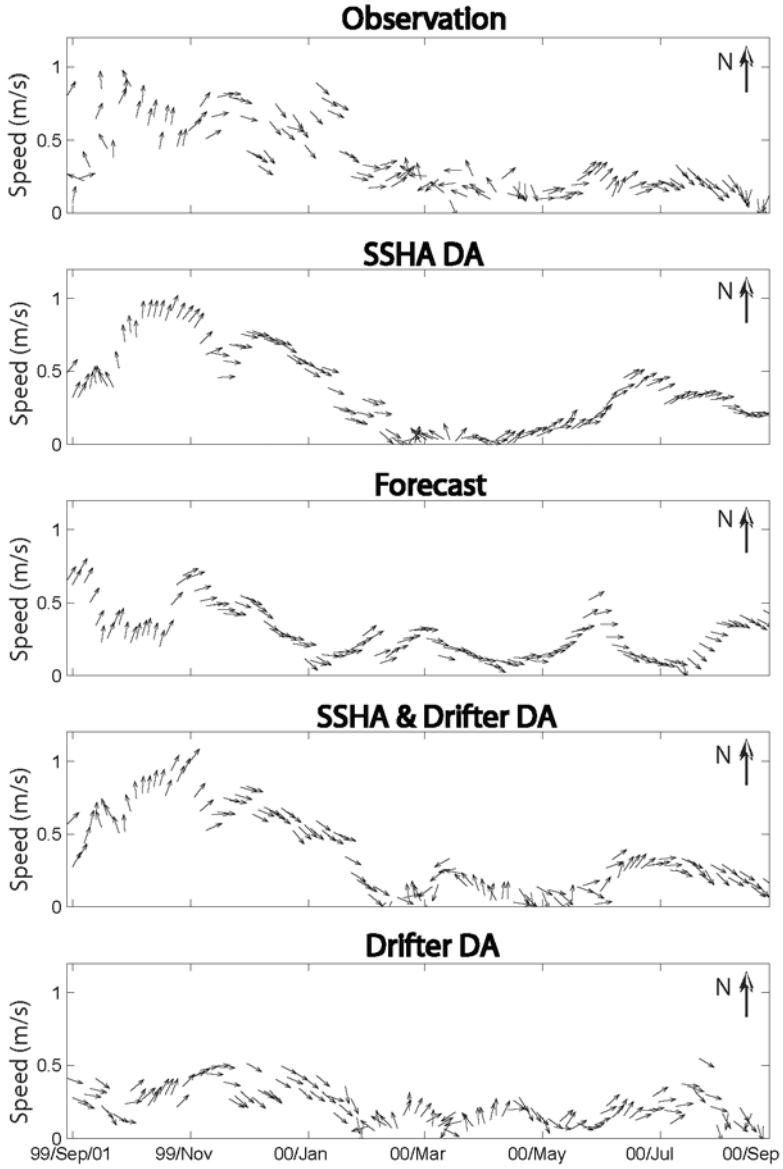

Figure 15. A comparison of ADCP velocity at the Sigsbee mooring at $z = -106$ m ("observation;" see Figure 3 for location) with the four indicated model experiments. Each velocity is plotted as a constant length arrowed vector that indicates direction, and the ordinate value of its tail indicates speed. The abscissa is time from 01 September 1999 through 14 September 2000.

and θ_{CC} (Drifter-only) is reduced, to 0.78 and $-15°$, respectively. With SSHA-DA, A_{CC} (SSHA-DA) $\approx$0.77 and θ_{CC} (SSHA-DA) $\approx$6.7°. Thus SSHA-DA further decreases the angle error, but the correlation remains similar to the Drifter-only analysis. On the other hand, Figure 13 indicates that the SSHA-DA analysis gives a better match to observations especially in the speeds, so that another measure of error in terms of the mean and Std errors is described below. Finally, the best agreement is obtained when both SSHA and drifters are assimilated, when A_{CC} (SSHA + Drf-DA) $\approx$0.86 and θ_{CC} (SSHA + Drf-DA) $\approx$ 4.3°.

[30] The mean and Std errors of speed and direction (Table 3) confirm that SSHA + Drf-DA produce the most accurate analysis currents along the ship track, with (u, v) errors of about 0.01±0.2 m s^{-1} in speed and 5 ± 50° in direction. These correspond to 2−14% of the observed means and are also well within the observed Stds ($R_{std} \approx$ 0.7). The quality of the analysis degrades as less data are assimilated, from SSHA + Drf-DA to SSHA-DA, to Drifter-only, and finally the forecast. For the SSHA-DA analysis, the (u, v) errors are 0.05±0.2 m s^{-1} in speed and 9±67° in direction, corresponding to 10−26% of the observed means, but an Std error in direction that is barely within the observed Std, $R_{std} \approx 0.9$. The improvements in the analysis currents when drifters are assimilated (in addition to SSHA-DA) are therefore quite significant. We should also mention that the drifter nudging scheme (Drf-DA1) also improves the analysis when combined with

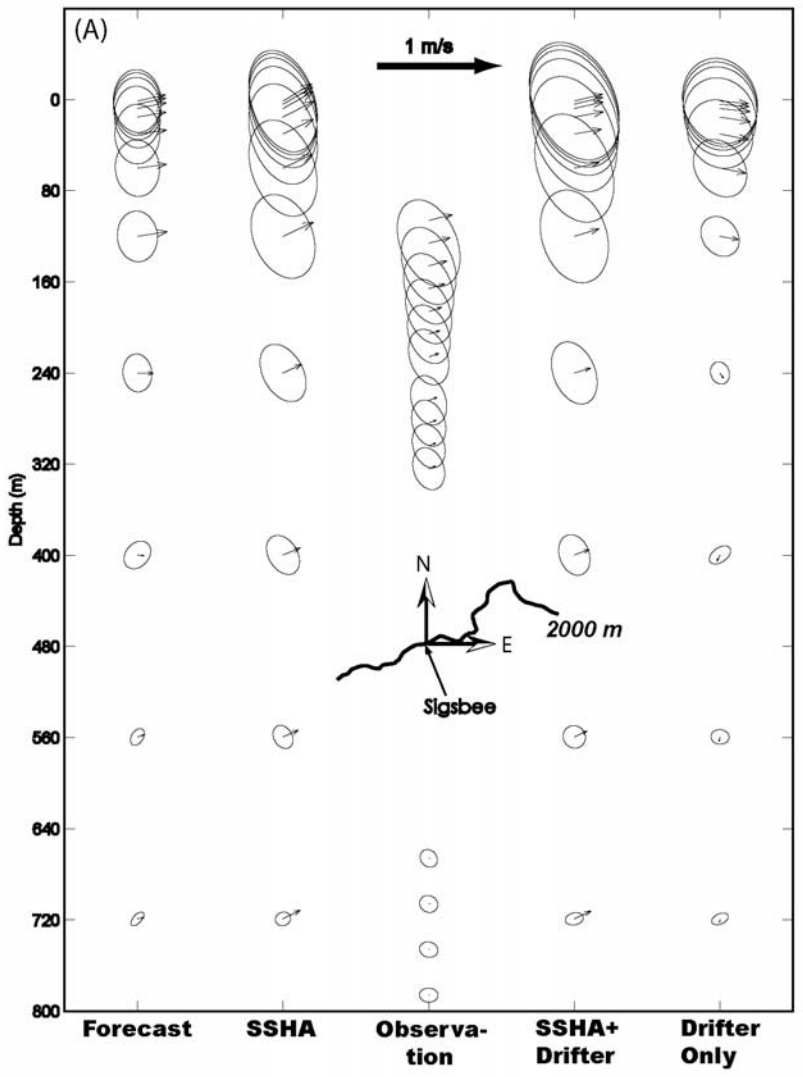

Figure 16. (a) Observed and model mean velocity vectors and principal axis standard deviation ellipses displayed as a function of depth ($z > -800$ m) at the Sigsbee mooring; the period of analysis is September 1999 through September 2000. Inset indicates Sigsbee mooring at the 2000-m isobath. (b) Plots of the corresponding semimajor and semiminor axes and also the principal axis angles. Breaks in observation line indicate missing data.

SSHA-DA, but the effect is less. The Lagrangian scheme (Drf-DA3) with SSHA-DA gives similar results as the SSHA + Drf-DA shown in Table 3.

7. Skill Assessments Against 1-Year ADCP at the Sigsbee Mooring

[31] The Sigsbee mooring is located near the region of high concentration of drifter data (Figure 3) and therefore provides an independent check of the skill of the analyses with or without drifter assimilations. Water depth is 2000 m, but the analysis will be in the upper layer ($z > \approx -800$ m), in three ranges where there are observations (section 3): $-106\text{ m} \geq z \geq -234$ m, $-256\text{ m} \geq z \geq -336$ m and $-658\text{ m} \geq z \approx > -800$ m. Table 4 summarizes various errors and complex correlations (CC) between model and observed velocities at four selected depths. Figure 14 shows |CC| and θ_{CC} maps of the complex correlation between the observed current at Sigsbee and the SSHA-Drf-DA analysis currents in the central Gulf of Mexico. There is a good match between the two time series at Sigsbee, $|CC| \approx 0.85$ and $\theta_{CC} \approx 0$. The region of high correlation (>0.8) and small angles ($\pm 30^\circ$ or less) is about 50 km $\times$ 50 km, an area which is well resolved by the model grid sizes of about 5–7 km in this region. The good agreements extend to deeper levels $z = -320$ m, the lower limit of the upper ADCP (Table 4). Similar correlation maps are also examined for the other analyses (not shown). For SSHA-DA, the contours are similar to Figure 14 except that the region of high correlation (>0.8) is slightly smaller, = 0.8 at Sigsbee, and the angle is $+3.9^\circ$. For the drifter-only assimilation, the region of high correlation shrinks further, and at Sigsbee, the value

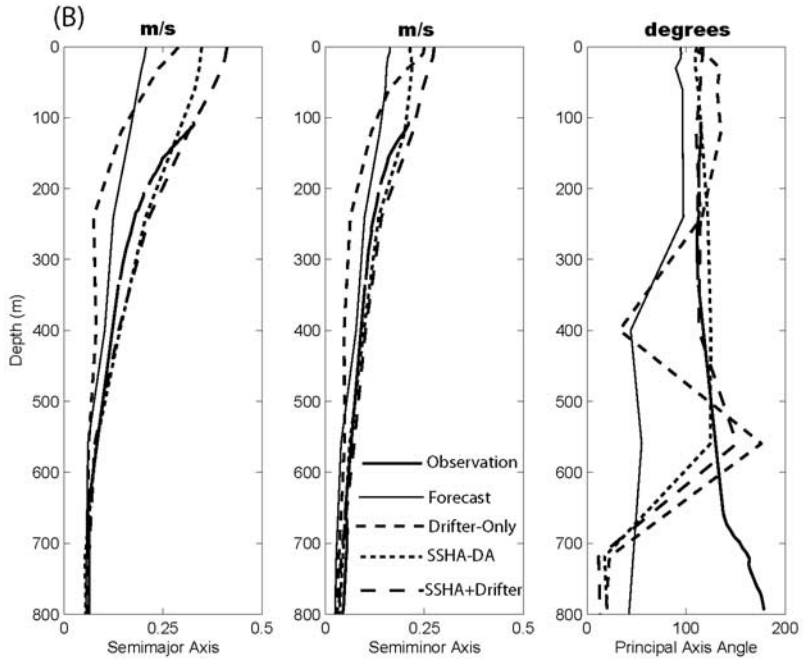

Figure 16. (continued)

decreases to 0.62 and the angle is $-10°$. For the forecast experiment, the correlation is = 0.55 and the angle is $-8°$.

[32] Figure 15 compares vector sticks at $z = -106$ m for the four analyses with the ADCP observation for the entire 1-year period. During the first 4–5 months, the current is dominated by Eddy-J, as can be seen by sticks that first point northward in October 1999 as the newly separated eddy was east of the mooring. The sticks then point eastward then southward in November-December 1999 as the eddy drifted westward. Beyond January 2000, the current variability is caused by weaker (and smaller) mesoscale features. Some of the observed variability around March 2000 and also in July-September 2000 is missing from the SSHA-DA analysis but is present in the SSHA + Drf-DA analysis. By comparing the forecast, drifter-only, and SSHA-Drf-DA analyses, we can see the effects of drifters in adjusting the velocity. Note that although we only assimilate drifters very near the surface, our analysis scheme allows adjustments of the model's internal pressure fields, hence also changes in the subsurface. As will be shown shortly, the effects of assimilating drifters penetrate to $z \approx -300$ m.

[33] Figures 16a and 16b compares the vertical distributions of mean velocities and PAStd ellipses. These were calculated on the original model and ADCP grids (i.e., no interpolation), but for clarity, not all are shown (the wide gaps $z \geq -106$ m and -336 m $\geq z \geq -658$ m are missing data; section 3). The SSHA-DA and SSHA + Drf-DA analyses, the mean, variances, semimajor/semiminor axes and principal axes angles throughout most of the upper layer -600 m $< z < -100$ m are in good agreements with the observations. The analyses show slightly more energetic currents for -400 m $< z < -100$ m and also larger means at $z = -720$ m, but the variances agree well with those observed at deeper levels. The observed variance shows an increasing trend toward the surface ($z > -100$ m), a fact that also exists in the analyses. (This increased variance has also been confirmed with a shorter ~3-month analysis of the observation near the surface.) The variances are less for the analysis that assimilates drifters only and also for the forecast, although the drifter assimilative analysis produces slightly larger variance near the surface.

[34] Finally, we compare observed and modeled empirical orthogonal function (EOF) modes. It turns out that the results are very similar whether we compute the EOFs on the model grid or we first interpolate the model velocities onto the ADCP grid. Here we show the latter. We wish to know the energy partition for the leading modes, and how their vertical structures and modal time series compare with those derived from the ADCP data. EOF modes are not dynamical modes; however, similarities of modes can indicate how well the observed variability is reproduced in the analyses. The observed partition of the three leading modes is 0.68:0.28:0.02. This is comparable to the partition 0.65:0.25:0.08 for the SSHA-DA analysis and 0.63:0.27:0.06 for the SSHA + Drf-DA analysis. Drifters tend to produce less organized motions and a narrower spread between modes 1 and 2, and the partition for the drifter-only analysis is 0.51:0.38:0.05. Partition for the forecast is 0.59:0.32:0.04.

[35] The eigenfunctions are compared in Figure 17. They show good agreements in the first two modes between either the SSHA-DA or SSHA + Drf-DA analysis and observation. The agreements with the drifter-only assimilative analysis and with the forecast are fair. The observed modes 1 and 2 are strongest near the surface and diminish rapidly with depth, becoming rather small for depths below about 300 m. (Model modes are stronger very near the surface; not shown.) Mode 1 (2) represents primarily cross

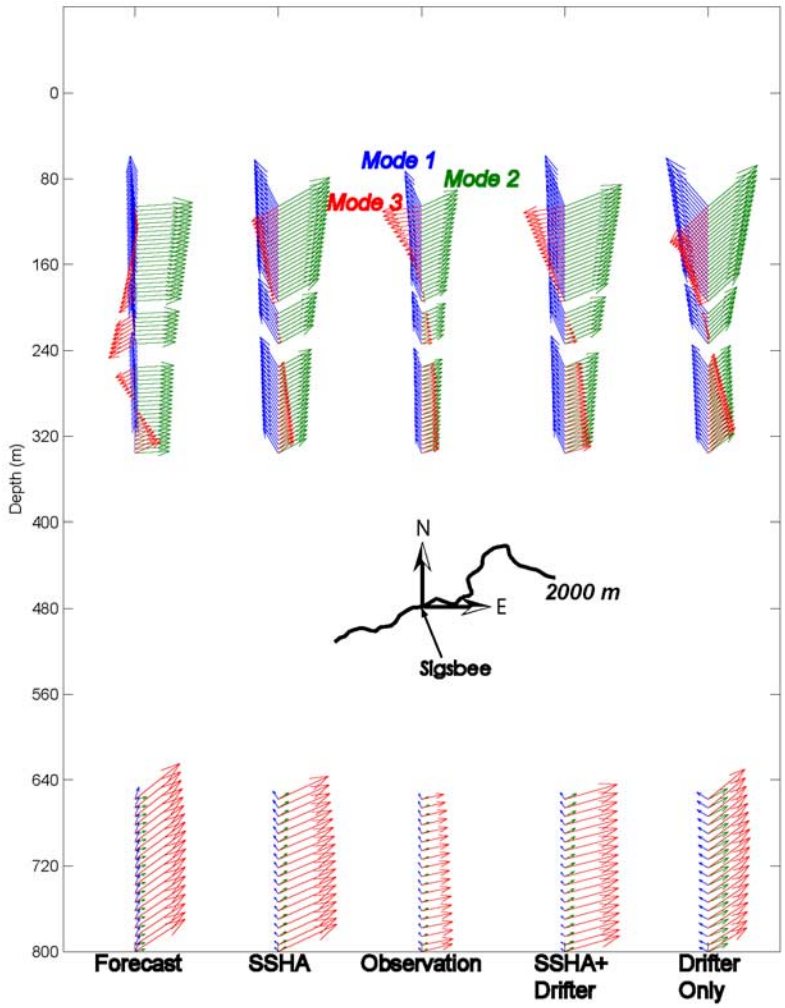

Figure 17. Vertical structures (i.e., eigenfuntions) of the three leading EOF modes for the indicated data-assimilative analyses and forecast experiment, as well as for the observation at the Sigsbee ADCP mooring. The period of analysis is September 1999 through September 2000. Inset indicates Sigsbee mooring at the 2000-m isobath.

(along-)-isobath motions; the modal time series are given in Figure 18, which shows that they are out of phase by approximately $\pi/2 \sim \pi$. They represent the dominant influence of Eddy-J as it began to separate from the loop current in September-October 1999, then rotated clockwise, and propagated westward pass the Sigsbee mooring during the next 3–4 months. (Reconstruction of these events using only the first two modes confirms the scenario; it is not shown here.) Variations in the remaining 7–8 months are less energetic and reflect the effects of weaker and smaller eddies. Apart from the energetic bursts of shorter period (~2 weeks) motions at the beginning (September-October 1999; cf., *Hamilton and Lugo-Fernandez*, 2001), Figure 18 shows that modes 1 and 2 of SSHA-DA and SSHA + Drf-DA analyses capture well the slower observed variations from September 1999 through February 2000. The agreements are not as good in the remaining period (of weaker variations), though inclusion of drifters (i.e., the SSHA + Drf-DA analysis) improves the match (March-April and mid-July 2000). Table 5 confirms that correlations between observed and model mode 1 for SSHA-DA and SSHA + Drf-DA are high especially for the first 6 months. For SSHA + Drf-DA, the correlation remains high also in the second 6 months. Note that the mode 1 correlation for the drifter-only assimilative experiment in the second 6 months is significantly higher than the SSHA-DA experiment. In the vicinity of the Sigsbee mooring, smaller scale eddies dominate during the second 6 months. Drifters appear to have captured this small-scale variability. Table 5 shows that the mode 2 correlations are not as high (as the mode 1 correlations), though SSHA + Drf-DA consistently outperforms the SSHA-DA analysis.

[36] The observed mode 3 consists of high-frequency motions (periods ≈ 10–20 days) and reversing eigenvector profile in the vertical (Figure 17). Mode 3 becomes relatively more important with depth, and there is also a tendency for near-bottom intensification (not shown). Although mode 3s from the analyses and forecast are also of high frequency and reversing vertical profiles, there is little correlation between any of them with the observation.

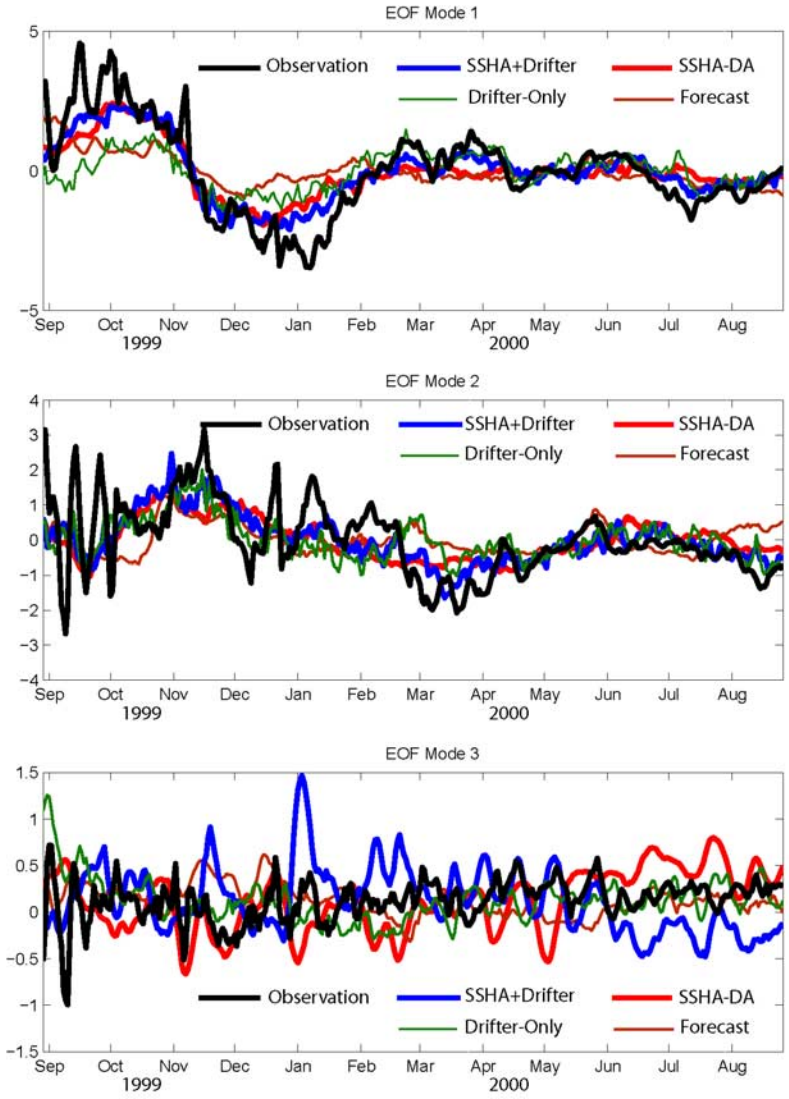

Figure 18. Temporal variations of the three leading EOF modes for the indicated data-assimilative analyses and forecast experiment, as well as for the observation at the Sigsbee ADCP mooring.

Near the bottom (not shown), mode 3 may be related to the presence of topographic Rossby waves (TRW) discussed by *Hamilton and Lugo-Fernandez* [2001]. *Oey and Lee* [2002] suggest that these waves are forced by small-scale meanders (<100 km) around the edges of the loop current and eddies. The TRW generation and propagation are therefore sensitive to details of the meanders, which are very difficult to model accurately.

8. Summary

[37] In this paper, we describe data-assimilative analyses on an ocean model that simulates loop current and eddies in the Gulf of Mexico, for the period August 1999 to September 2000. Data used in the analyses are altimetry SSHA and surface drifters. Sequential assimilations with statistical interpolation schemes are tested. The goal is to quantify in an eddy-rich ocean environment the accuracy of currents obtained from a model that assimilates altimetry sea-surface height anomaly (SSHA) data and surface drifters; we wish to know how drifters can improve the analyses. To the best of our knowledge, model skill assessment study of chaotic eddies has never been previously conducted in the Gulf of Mexico. Experiments initialized with the same field, with and without altimetry and/or drifter assimilations, including a forecast case (without assimilation) for comparison, are conducted.

Table 5. Correlation Coefficients Between Observed and Model EOF Modes 1 and 2[a]

	EOF Mode 1			EOF Mode 2		
Model Experiments	Year	1st 6 mo.	2nd 6 mo.	Year	1st 6 mo.	2nd 6 mo.
Forecast	0.64	0.73	0.43	*0.24*	*0.23*	*0.13*
Drifter Only	0.69	0.73	0.74	0.51	0.44	*0.34*
SSHA-DA	0.88	0.92	*0.41*	0.50	*0.24*	0.58
SSHA + Drf-DA	0.93	0.94	0.83	0.63	*0.34*	0.69

[a]Year = September 1999 through August 2000; 1st 6 months = September 1999 through February 2000 and 2nd 6 months = March-August 2000. Italicized numbers are values below the 99% significance level.

[38] The results are first checked against the SSHA and drifter data. It is shown that assimilating altimetry SSHA alone results in a good overall match between the analysis and observed (drifter-derived) surface currents in the Gulf. The average speed errors ≈8% of observed, direction errors $\approx -1 \pm 25^\circ$ and the amplitude of complex correlations, $|CC| \approx 0.6$ with small angle $|\theta_{CC}| \approx 1^\circ$ (Figure 11; Table 2). The clearest evidence of improved analyses when drifters are assimilated is from comparing the pure forecast case with the analysis that assimilates only drifters. The latter is shown to sufficiently constrain the pressure field that the analyzed loop current and eddies match fairly well their behaviors inferred from satellite altimetry data (e.g., Figure 7). The drifter-derived SSHAs significantly correlate with altimetry data (coefficient >0.5) over several months (Figure 6) and in a large portion of the Gulf (Figure 5). We see from equation (5) that, even though drifters are assimilated only near the surface, SSHAs are altered through the perturbed (drifter-derived) velocities.

[39] Model results are next evaluated against ships and moored ADCPs. Assimilating drifters in addition to SSHA consistently improve the upper −100 m analysis: $|CC| \approx 0.85-0.88$, $|\theta_{CC}| < 4^\circ$, and mean speed errors ≈ 1–2%. The standard deviation errors in speeds and directions are well within the observed standard deviations. The good agreements extend to $z \approx 300$ m where $|CC| \approx 0.74$ and $|\theta_{CC}| \approx 6^\circ$. The energy partition of the first three observation EOF (-800 m $\leq z \leq 106$ m) modes at the Sigsbee mooring is 0.68:0.28:0.02. The dominant modes 1 and 2 are vertically coherent but strongly sheared and represent energetic eddies that propagate past Sigsbee, with timescales from weeks to months. On the other hand, mode 3 has timescales of 10–20 days, a reversing vertical profile, and intensifies for $z < -300$ m. It probably represent meanders that develop around larger eddies and the loop current. Modes 1 and 2 of EOFs obtained from both SSHA-DA and SSHA + Drf-DA analyses agree well with those observed in terms of energy partitions and vertical profiles of eigenfunctions. Mode 1 temporal variation also agrees well with the observation. Mode 2 time series compares less favorably with the observation, though including drifters in the assimilation (i.e., SSHA + Drf-DA) improves the results. Since altimetry data already include some of the surface-current information contained in the drifter data, improved analyses (by also assimilating drifters) tend to occur at ocean sites where currents are not dominated by large-scale eddies, i.e., where altimetry data are less effective. This is so for example at Sigsbee during the second half of the 1-year analysis period. The correlation analyses of the EOF modes (Table 5), for example, demonstrate this. The forecast mode 1 shows some agreement with observation mode 1, suggesting that the model has inherent predictability [cf., *Oey et al.*, 2005a].

[40] The type of (i.e., simple) data assimilation schemes tested here is widely used in operational models of mesoscale ocean currents and eddies. In recent years, the trend is toward the development of sophisticated schemes that include, for example, more accurate estimates of the error covariance (e.g., 4DVAR scheme; *Kalnay*, 2003). We have shown here that the 'simpler' schemes can provide accurate solutions in the sense of small errors when compared against independent observations; at Sigsbee for example, Table 4 gives %errors ≈ 1, $|CC| \approx 0.85$ and $\theta_{CC} \approx 0.3^\circ$. Future plans include using more sophisticated assimilation schemes; it will be a challenge then to further improve the present analysis. A natural extension of the present work is to conduct forecast experiments that test if the improved analysis with drifters leads also to improved forecasts.

Appendix A: Complex Correlation (CC)

[41] The "CC" between two velocity time series $\mathbf{u}_1 = (\mathbf{u}_1, v_1)$ and $\mathbf{u}_2 = (\mathbf{u}_2, \mathbf{v}_2)$, is defined as [*Kundu*, 1976]:

$$CC = \langle \mathbf{w}_1 \mathbf{w}_2^* \rangle / \left[\langle \mathbf{w}_1 \mathbf{w}_1^* \rangle^{1/2} \langle \mathbf{w}_2 \mathbf{w}_2^* \rangle^{1/2} \right], \tag{A1}$$

where $w_n = u_n + iv_n$, $n = 1, 2$, $i = (-1)^{1/2}$, the asterisk indicates the complex conjugate, and $\langle . \rangle$ denotes time averaging. *Kundu* [1976] was interested in the veering angle between $\mathbf{u}_1$ and $\mathbf{u}_2$ in the bottom Ekman layer and showed that the phase of CC, θ_{CC}, is the average veering angle (between the two vectors) weighted by the speeds of the instantaneous vectors. For the present case, CC measures how closely the model vector $\mathbf{w}_1$ follows the observation vector $\mathbf{w}_2$ in their indexed space, which can be the spatial dimension (as with regionwide observations considered as being a snapshot), time (as in time series of moored data), or both space and time (as in drifters). Clearly, θ_{CC} should be small for the two vectors to be 'close,' but $|CC|$ should also be high ($|CC|$ is < 1 from (A1)). By considering simple sinusoids, it can be shown that $|CC|$ is small if $\mathbf{u}_1$ and $\mathbf{u}_2$ have disparate frequencies. For similar frequencies $|CC| \approx \cos(\phi)$, where ϕ is the (average) phase-shift between $\mathbf{u}_1$ and $\mathbf{u}_2$. On the other hand, θ_{CC} is independent of ϕ, so that it is possible for $|CC| = 1$ but $\theta_{CC} = 90^\circ$ and vice versa for $|CC| = 0$ but $\theta_{CC} = 0$. The behavior of CC is more complicated for general time series. The upshot is, for the model analysis to be any good, we require $|CC| \approx 1$ and $\theta_{CC} \approx 0$.

[42] **Acknowledgments.** This study is supported by the Minerals Management Service (MMS) under contract #1435-01-04-CT-35279. The Sigsbee portion of the research is supported by MMS contract #1435-01-05-CT-39053. LYO appreciates the inputs and encouragements of Program Managers Drs. Walt Johnson and Alexis Lugo Fernandez. Computing was conducted at GFDL/NOAA.

References

Anderson, D. L. T., J. Sheinbaum, and K. Haines (1996), Data assimilation in ocean models, *Rep. Prog. Phys.*, *59*, 1209–1266.

Awaji, T., N. Imasato, and H. Kunishi (1980), Tidal exchange through a strait: A numerical experiment using a simple model basin, *J. Phys. Oceanogr.*, *10*, 1499–1508.

Bennett, A. F. (2002), Inverse modeling of the ocean and atmosphere, Cambridge Univ. Press, New York, 234 pp.

Chen, C., R. O. Reid, and W. D., Nowlin Jr. (1996), Near-inertial oscillations over the Texas-Louisiana shelf, *J. Geophys. Res.*, *101*, 3509–3524.

Daley, R. (1991), *Atmospheric Data Analysis*, Cambridge Univ. Press, New York, 457 pp.

DiMarco, S. F., W. D., Nowlin Jr., and R. O. Reid (2005), A Statistical Description of the Velocity Fields from Upper Ocean Drifters in the Gulf of Mexico. In "Circulation in the Gulf of Mexico: Observations and Models," W. Sturges and A. Lugo-Fernandez Eds, *Geophysical Monograph Series,* Vol.161, 360 pp.

Ducet, N., P. Y. Le Tron, and G. Reverdin (2000), Global high-resolution mapping of ocean circulation from TOPEX/Poseidon and ERS-1 and -2, *J. Geophys. Res.*, *105*, 19,477–19,498.

Ezer, T., and G. L. Mellor (1994), Continuous assimilation of Geosat altimeter data into a three-dimensional primitive equation Gulf Stream model, *J. Phys. Oceanogr.*, *24*(4), 832–847.

Ezer, T., L.-Y. Oey, W. Sturges, and H.-C. Lee (2003), The variability of currents in the Yucatan Channel: Analysis of results from a numerical ocean model, *J. Geophys. Res.*, *108*(C1), 3012, doi:10.1029/2002JC001509.

Fan, S.-J., L. Y. Oey, and P. Hamilton (2004), Assimilation of drifters and satellite data in a circulation model of the northeastern Gulf of Mexico, *Cont. Shelf Res.*, *24*(9), 1001–1013.

Fratantoni, D. M. (2001), North Atlantic surface circulation during the 1990's observed with satellite-tracked drifters, *J. Geophys. Res.*, *106*, 22,067–22,093.

Garvine, R. W. (1999), Penetration of buoyant coastal discharge onto the continental shelf: A numerical model experiment, *J. Phys. Oceanogr.*, *29*, 1892–1909.

Hamilton, P. (1992), Lower continental slope cyclonic eddies in the central Gulf of Mexico, *J. Geophys. Res.*, *97*, 2185–2200.

Hamilton, P., and A. Lugo-Fernandez (2001), Observations of high speed deep currents in the northern Gulf of Mexico, *Geophys. Res. Lett.*, *28*, 2867–2870.

Hamilton, P., G. S. Fargion, and D. C. Biggs (1999), Loop current eddy paths in the western Gulf of Mexico, *J. Phys. Oceanogr.*, *29*, 1180–1207.

Hamilton, P., J. J. Singer, E. Waddell, and K. Donohue (2003), Deepwater observations in the northern Gulf of Mexico from in-situ current meters and PIES. Final Report. Volume II: Technical Report. U.S. Dept. of the Interior, Minerals Management Service, Gulf of Mexico OCS Region, New Orleans, LA. OCS Study MMS 2003-049.95pp.

Isaacson, E., and H. B. Keller (1966), Analysis of Numerical Methods, John Wiley and Sons New York, 541 pp.

Kalnay, E. (2003), Atmospheric modeling, data assimilation and predictability, Cambridge Univ. Press, New York, 341 pp.

Kamachi, M., et al. (2004), Short-range prediction experiments with operational data assimilation system for the Kuroshio south of Japan, *J. Oceanogr. Soc. Jpn*, *60*, 269–282.

Kundu, P. (1976), An analysis of inertial oscillations observed near Oregon coast, *JPO*, *6*, 879–893.

Mellor, G. L. (2004), Users guide for a three-dimensional, primitive equation, numerical ocean model. Program in Atmospheric and Oceanic Sciences, Princeton Univ. Press, 42 pp.

Mellor, G. L., and T. Ezer (1991), A gulf stream model and an altimetry assimilation scheme, *J. Geophys. Res.*, *96*, 8779–8795.

Mellor, G.-L., T. Ezer, and L. Y. Oey (1994), The pressure gradient conundrum of sigma coordinate ocean models, *J. Atmos. Oceanic Tech.*, *11*, 1126–1134.

Merrifield, M. A., and R. T. Guza (1990), Detecting propagating signals with complex empirical orthogonal functions: A cautionary note, *J. Phys. Oceanogr.*, *20*, 1628–1633.

Miyazawa, Y., S. Yamane, X. Guo, and T. Yamagata (2005), Ensemble forecast of the Kuroshio meandering, *J. Geophys. Res.*, *110*, C10026, doi:10.1029/2004JC002426.

Molcard, A., L. I. Piterbarg, A. Griffa, T. M. Ozgokmen, and A. J. Mariano (2003), Assimilation of drifter observations for the reconstruction of the Eulerian circulation field, *J. Geophys. Res.*, *108*, (C3), 3056, doi:10.1029/2001JC001240.

Nowlin, W. D., Jr., A. E. Jochens, S. F. DiMarco, R. O. Reid, and M. K. Howard (2001), Deepwater physical oceanography reanalysis and synthesis of historical data: Synthesis Report, OCS Study MMS 2001-064, 528 pp., U.S. DOI, MMS, Gulf of Mexico OCS Region, New Orleans, Louisiana.

Oey, L.-Y. (2004), Vorticity flux in the Yucatan Channel and loop current eddy shedding in the Gulf of Mexico, *J. Geophys. Res.*, *109*, C10004, doi:10.1029/2004JC002400.

Oey, L.-Y., and P. Chen (1992), A model simulation of circulation in the north-east Atlantic shelves and seas, *J. Geophys. Res.*, *97*, 20,087–20,115.

Oey, L.-Y., and H.-C. Lee (2002), Deep eddy energy and topographic Rossby waves in the Gulf of Mexico, *JPO*, *32*, 3499–3527.

Oey, L.-Y., and H.-C. Zhang (2004), A mechanism for the generation of subsurface cyclones and jets, *Cont. Shelf Res.*, *24*, 2109–2131.

Oey, L.-Y., H.-C. Lee, and W. J. Schmitz Jr. (2003a), Effects of winds and Caribbean eddies on the frequency of loop current eddy shedding: A numerical model study, *J. Geophys. Res.*, *108*(C10), 3324, doi:10.1029/2002JC001698.

Oey, L.-Y., P. Hamilton, and H.-C. Lee (2003b), "Modeling and data-analyses of circulation processes in the Gulf of Mexico." Final Report to the Minerals Management Service, Contract #1435-01-99-CT-31028; 116 pp, 56 figures. Available from http://www.gomr.mms.gov/PI/PDFImages/ESPIS/2/3046.pdf.

Oey, L.-Y., T. Ezer, and T. Sturges (2004), Modeled and observed empirical orthogonal functions of currents in the Yucatan Channel, *J. Geophys. Res.*, *109*, C08011, doi:10.1029/2004JC002345.

Oey, L.-Y., T. Ezer, G. Forristall, C. Cooper, S. DiMarco, and S. Fan (2005a), An exercise in forecasting loop current and eddy frontal positions in the Gulf of Mexico, *Geophys. Res. Lett.*, *32*, L12611, doi:10.1029/2005GL023253.

Oey, L.-Y., T. Ezer, and H. J. Lee (2005b), Loop current, rings and related circulation in the Gulf of Mexico: A review of numerical models and future challenges. In "Circulation in the Gulf of Mexico: Observations and Models," W. Sturges and A. Lugo-Fernandez Eds, Geophysical Monograph Series, Vol. 161, 360 pp.

Oey, L.-Y., T. Ezer, D.-P. Wang, S. Fan, and X.-Q. Yin (2006a), Loop current warming by hurricane Wilma, *Geophys. Res. Lett.*, *33*, L08613, doi:10.1029/2006GL025873.

Oey, L.-Y., T. Ezer, D.-P. Wang, X.-Q. Yin, and S.-J. Fan (2006b), Hurricane-induced motions and interaction with ocean currents, *Cont. Shelf Res.*, in press. (Available from http://www.aos.princeton.edu/WWWPUBLIC/PROFS/publications.html)

Ohlmann, J. C., P. P. Niiler, C. A. Fox, and R. R. Leben (2001), Eddy energy and shelf interactions in the Gulf of Mexico, *J. Geophys. Res.*, *106*, 2605–2620.

Oke, P., et al. (2002), A modeling study of the three-dimensional continental shelf circulation off oregon: Part I. Model-data comparisons, *J. Phys. Oceanogr.*, *32*, 1360–1382.

Ozgokmen, T. M., A. Molcard, T. M. Chin, L. I. Piterbarg, and A. Griffa (2003), Assimilation of drifter observations in primitive equation models of midlatitude ocean circulation, *J. Geophys. Res.*, *108*(C7), 3238, doi:10.1029/2002JC001719.

Paduan, J. D., and I. Shulman (2004), HF radar data assimilation in the Monterey Bay area, *J. Geophys. Res.*, *109*, C07S09, doi:10.1029/2003JC001949.

Reid, R. O., and R. E. Whitaker (1981), Numerical model for astronomical tides in the Gulf of Mexico. Texas A and M report for U. S. Army Engineers Waterway Experiment Station, pp115.

Richardson, P. L. (2005), Caribbean Current and eddies as observed by surface drifters, *Deep Sea Res.*, *52*, 429–463.

Schmitz, W. J., Jr. (2005), Cyclones and westward propagation in the shedding of anticyclonic rings from the loop current. In "Circulation in the Gulf of Mexico: Observations and Models," W. Sturges and A. Lugo-Fernandez Eds, *Geophysical Monograph Series*, Vol. 161, 360 pp.

Sturges, W., and A. Lugo-Fernandez (Eds) (2005), Circulation in the Gulf of Mexico: Observations and Models. Geophysical Monograph Series, Vol. 161, 360 pp.

Vázquez de la Cerda, A. M., R. O. Reid, S. F. DiMarco, and A. E. Jochens (2005), Bay of Campeche Circulation: An Update. In "Circulation in the Gulf of Mexico: Observations and Models," W. Sturges and A. Lugo-Fernandez Eds, Geophysical Monograph Series, Vol. 161, 360 pp.

Walpert, J. N., N. L. Guinasso Jr., F. J. Kelly, L. L. Lee III, O. Wang, and S. DiMarco (2004), "1999 ADCP and XBT Surveys of Eddy Juggernaut in the Gulf of Mexico," Technical Report to EJIP by GERG, Texas A&M Univ., 727 Graham Rd., College Station, TX 77845.

Wang, D.-P., L.-Y. Oey, T. Ezer, and P. Hamilton (2003), Nearsurface currents in DeSoto Canyon, *JPO*, *33*, 313–326.

Yin, X-Q, and L-Y Oey (2007), Bred-ensemble ocean forecast of Loop Current and rings, *Ocean Modell.*, doi:10.1016/j.ocemod.2007.02.005.

X.-H. Lin and L.-Y. Oey, Princeton University, Atmospheric and Oceanic Sciences, Princeton University, PO Box CN 710, Sayre Hall, Forrestal Campus, Princeton, NY 08544, USA. (lyo@princeton.edu)

D.-P. Wang, Stony Brook University, Stony Brook, NY, USA.